PART I

MODES IN

SPHERICAL-MIRROR RESONATORS

PART II

DOMINANT MODE CALCULATIONS

IN OUTPUT-COUPLED

INFINITE STRIP MIRROR RESONATORS

Thesis by

Walter Albert Specht, Jr.

In Partial Fulfillment of the Requirements

For the Degree of

Doctor of Philosophy

California Institute of Technology

Pasadena, California

1965

(Submitted May 10, 1965)

ACKNOWLEDGEMENTS

The aid and encouragement given to me by my advisor, Dr. Nicholas A. George, has been of immeasurable value to this work and to myself.

The interest and efforts of Drs. Jon Mathews, Charles H. Papas, Robert V. Langmuir, Peter O. Clark, Donald H. Close, and Mr. Andrew Dienes in the theoretical and mathematical aspects of this work are very much appreciated. The computer calculations benefited from the programs and attention of Dr. Klaus W. Jacob, Miss Kikuko Matsumoto, and Mrs. Martha L. Lamson.

The financial assistance of the Corning Glass Works Fellowship in 1960-1961 and the Howard Hughes Doctoral Fellowship in 1961-1965 is gratefully acknowledged.

My thanks go to Mrs. Olive List for typing this work, and to Miss Kay Balderson for drawing the figures.

ABSTRACT

PART I

This work is the examination of a cavity mode approach to the mode structure of a laser. Solutions of the vector wave equation for electromagnetic fields in and between perfectly conducting oblate spheroidal cavities are examined for the case of wavelengths much less than cavity dimensions. These solutions are the field modes in Fabry-Perot type resonators with equal-radius concave spherical mirrors, or with concave-convex spherical mirrors, when the parameters of the oblate spheroids are chosen so that the radii of curvature and spacing on the axis of rotation match those of the resonator mirrors. Expressions for the transverse and longitudinal mode structures are derived. The eigenvalue equations are written, and are solved for the case of the two lowest order modes.

PART II

This work is the numerical calculation of the steady state lowest order even and odd symmetry electromagnetic field patterns at the mirrors of the multimode resonator formed by two plane-parallel infinite strip mirrors, modified for output coupling by central strips of zero reflectivity. The equation solved is the scalar Huyghens-Fresnel integral equation (a transverse electromagnetic wave approximation to the vector integral equation, valid when the wavelength is much less than the cavity dimensions) relating the fields at the two mirrors, converted to an eigenvalue equation, and approximated for calculations by a matrix eigenvalue equation. The mode structure, power loss and phase shift per transit, and output coupling are discussed.

TABLE OF CONTENTS

PART I

MODES IN

SPHERICAL-MIRROR RESONATORS

CHAPTER ONE

INTRODUCTION

1.1 Review of the Field

The development of coherent light sources has opened the optical regions of the electromagnetic spectrum for use in communication systems, just as the radio transmitter made communication systems possible at the longer wavelengths. As a result, it is of interest to consider the extension of the techniques and devices now used at radio frequencies into the optical region.

One device of interest is the optical resonator. It is receiving current application both as a passive filter and as the resonant element in a laser oscillator or amplifier. In long-distance communications the problem of optical beam guiding is important.

In this work the passive resonator is analyzed as a boundary value problem in electromagnetic theory, and additional complex configurations are treated computationally. These results have application to the beam guiding system also.

Schawlow and Townes (1), Prokhorov (2), and Dicke (3), having recognized the need for low loss resonators, suggested the use of Fabry-Perot interferometers as multimode optical resonators. The self-consistent field calculations of Fox and Li (4) showed that this resonator could support so-called "normal" modes, that is, modes that reproduced themselves to within a constant factor when bounced from one mirror to the other.

The use of two confocal spherical mirrors as an interferometer had been previously discussed by Connes (5,6). Fox and Li (4) also made numerical calculations on this resonator and showed that its diffraction loss is orders of magnitude less than that of a plane-parallel mirrors resonator. Boyd and Gordon (7) analytically solved the problem of mode structure in this resonator, and Boyd and Kogelnik (8) extended this analysis to non-symmetric confocal resonators. Goubau and Schwering (9), Deschamps and Mast (75), and Tien et al. (76) have considered the optical beam transmission guide with periodic phase correction; some of their results are applicable to laser resonators with spherical mirrors. Numerical calculations on non-confocal resonators were carried out by Fox and Li (10,11) and by Soohoo (12), using the method of self-consistent field reproduction. Numerical calculations by the kernel expansion-truncation technique have been carried out by She and Heffner (13) and by Bergstein and Schachter (14) for the plane-parallel mirrors resonators. She and Heffner have also shown that the results are applicable to a spherical sector resonator. McCumber (15) has used this technique to calculate the modes of confocal resonators, including the effects of output-coupling apertures on the mirrors.

Kotik and Newstein (16) and Barone (17) have considered the cavity mode problem by using superposition of plane wave spectra. Vainshtein (18) has used the consideration of diffraction at the open end of a waveguide to analyze the plane-parallel mirrors resonator, and the parabolic equation method to analyze the non-confocal spherical mirrors resonator (19), the plane-parallel mirrors resonator and open

waveguides with plane mirrors (20), and cylindrical mirrors (21). Clark (22) has analyzed the mode structure within multimirror cavities, where bounces off several mirrors are required to return a beam to its starting point.

A physical system is approximated by an idealized mathematical model for the purpose of analyzing its fundamental characteristics. The real system is never ideal, so that perturbations on the results of the mathematical analysis must be considered. Asmus (23) has carried out an analysis of the effects of imperfect figure, polish and alignment of the mirrors on the optical maser performance of a confocal resonator. Fox and Li (10) have made calculations on the effects of tilt on plane-parallel mirrors resonators. Observations of the effect of imperfections in the coatings of multilayer dielectric film mirrors, a type of perturbation not so far treated, have been made (see Appendix D).

1.2 Content of this Paper

Boyd and Gordon (7) analytically solved the problem of the mode structure in a Fabry-Perot type resonator with two identical, square cross-section spherical mirrors by the application of the Huyghens-Fresnel principle, relating the field at the "source" mirror to the field at the "field point" mirror, and by requiring that the fields at the two mirrors be identical within an arbitrary complex constant. Boyd and Kogelnik (8) applied the same technique to resonators with mirrors of different cross-sections and different radii

of curvature. Several approximations were made in their analyses: the source-enclosing surface at the "source" mirror is not a closed surface, the vector integral equation is scalarized, the integration point to field point distance is approximated, and the normal derivative at the "source" mirror surface is approximated. That these approximations are valid at visual and infrared wavelengths has been widely demonstrated (24-26).

Another approach to the solution of the problem of laser mode structure can be seen if one considers that the reflectivity of practical resonator mirrors is nearly unity, and that the field strength of the modes described by Boyd and Gordon and by Boyd and Kogelnik is very small off the reflector axis for the visual and infrared wavelengths. It becomes clear that the mirrors can be assumed perfectly reflecting and can be continued laterally. Thus, the laser modes should be derivable from the modes of a totally enclosed cavity with perfectly conducting boundary walls having the shape of the resonator mirrors near the axis, as long as the mode field strength is small everywhere off the axis. It is natural, then, to consider an oblate spheroidal cavity. By suitable choice of the parameters defining an oblate spheroid, the portions of its surface near the axis of rotation will approximate the curvature and match the spacing of any set of equal-radius mirrors spaced closer than concentrically. A focusing convex-concave mirrors resonator system can be matched with the cavity between two confocal spheroids. (Though the plane-parallel mirror configuration and the concentrically spaced spherical mirror configuration are

limiting cases of the oblate spheroidal coordinate system, the requirement of small field strength off the axis is not met; and this approach is not useful for these cases.)

The vector wave equation is not generally separable in the spheroidal coordinate systems; boundary conditions are not easily matched (27,28). It is separable when the fields are restricted to rotational symmetry, so that rotational modes can be treated exactly. However, the forms of the general solutions of the vector wave equation are such that the boundary conditions can be approximately matched when the wavelength is small compared to the cavity dimensions.

The outline of this approach to the analysis of laser resonator modes has been given by Zimmerer (29). The detailed analysis consists of matching the spheroid(s) to the laser configuration, taking the solutions of the vector wave equation in oblate spheroidal coordinates, applying the perfectly conducting oblate spheroidal boundary conditions, and examining the solutions for their form in the case of wavelengths small compared to the cavity dimensions.

Vainshtein (20) has considered the laser resonator problem in oblate spheroidal coordinates from the approach of the parabolic equation method. His results are found more generally here. Ito (30) has also considered the laser resonator problem in oblate spheroidal coordinates.

CHAPTER TWO

OBLATE SPHEROIDAL COORDINATE SYSTEM

The oblate spheroidal coordinate system (see Figure 1) is a degenerate form of the generalized confocal ellipsoidal coordinate systems, in which the x and y axes intersect a given ellipsoid at equal distances from the origin and the z axis intersection is closer to the origin than the others. It can be generated by the rotation of a two-dimensional elliptical coordinate system about its minor axis. It is an orthogonal coordinate system related to the Cartesian coordinate system by the equations

$$x = \tfrac{1}{2} d\left[(1 - \eta^2)(\xi^2 + 1)\right]^{\frac{1}{2}} \cos\varphi$$

$$y = \tfrac{1}{2} d\left[(1 - \eta^2)(\xi^2 + 1)\right]^{\frac{1}{2}} \sin\varphi \qquad 2.1$$

$$z = \tfrac{1}{2} d\,\eta\xi$$

where the notation is that of Flammer (31), used throughout this paper. The coordinates x, y, and z are invariant under any change of signs of η and ξ such that the product $\eta\xi$ does not change sign. The coordinate ranges most useful to the present problem are

$$-1 \le \eta \le +1$$

$$0 \le \xi < \infty \qquad 2.2$$

$$0 \le \varphi \le 2\pi \quad ,$$

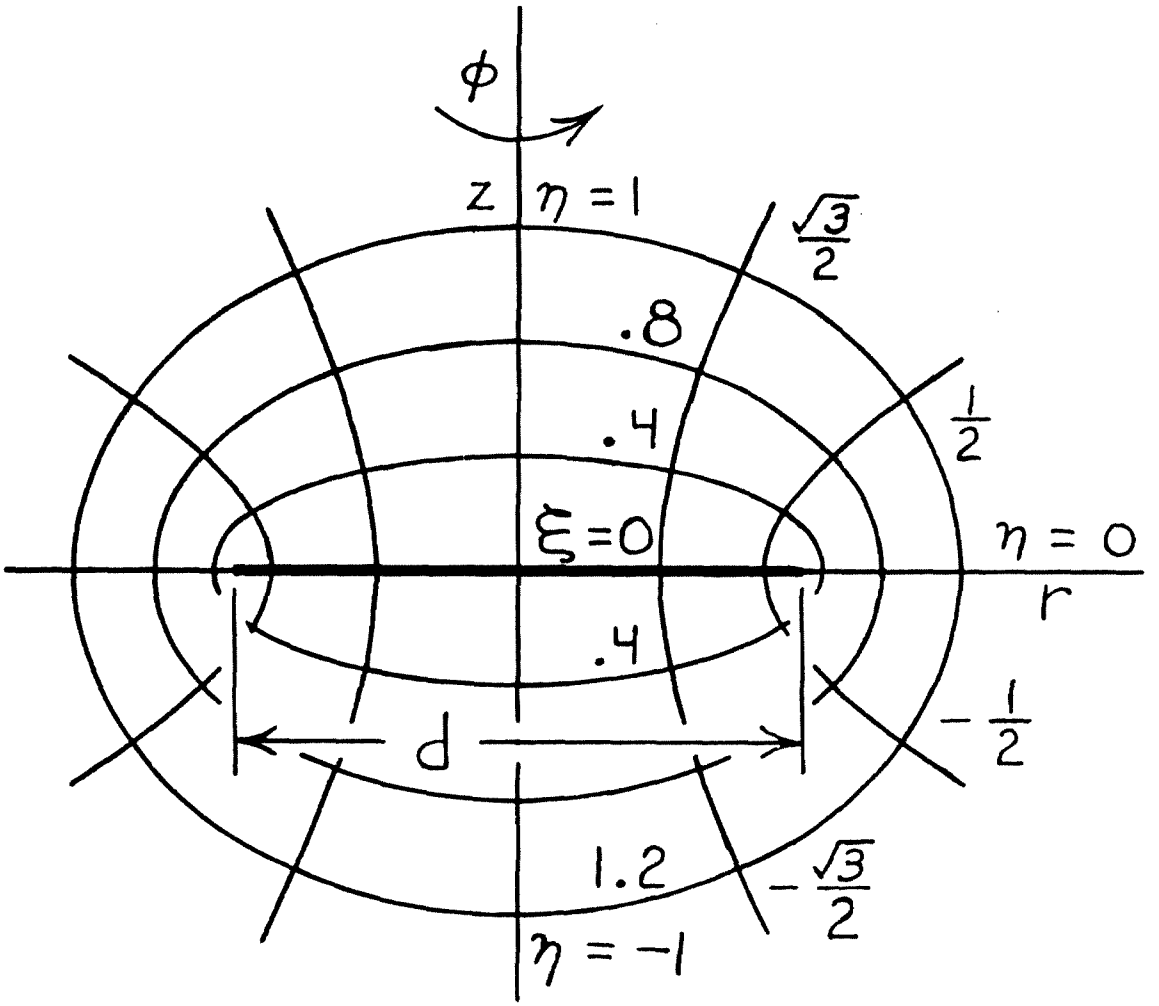

Figure 1. Oblate spheroidal coordinate system.

since the spheroidal surfaces are then given by the single value ξ . These coordinate ranges are shown in Figure 1.

Surfaces of constant η are hyperboloids of revolution of one sheet, surfaces of constant ξ are spheroids, and surfaces of constant φ are planes. The unit vectors $\bar{e}_\eta$, $\bar{e}_\xi$, $\bar{e}_\varphi$ form a right hand triple. The length of the infinitesimal vector ds is given by

$$ds^2 = h_\eta^2 \, d\eta^2 + h_\xi^2 \, d\xi^2 + h_\varphi^2 \, d\varphi^2 \qquad 2.3$$

where the scale factors h are given by

$$\begin{aligned} h_\eta &= \tfrac{1}{2} d\left[(\xi^2 + \eta^2)/(1 - \eta^2)\right]^{\frac{1}{2}} \\ h_\xi &= \tfrac{1}{2} d\left[(\xi^2 + \eta^2)/(\xi^2 + 1)\right]^{\frac{1}{2}} \qquad 2.4 \\ h_\varphi &= \tfrac{1}{2} d\left[(1 - \eta^2)\,(\xi^2 + 1)\right]^{\frac{1}{2}} \quad . \end{aligned}$$

CHAPTER THREE

CONNECTION BETWEEN LASER PARAMETERS AND EQUIVALENT SPHEROID PARAMETERS

3.1 Single Spheroidal Surface

Figure 2 defines the parameters ξ_0 and d of an oblate spheroid and the parameters a, b, and d of its generating ellipse. The two equations connecting these parameters are, from the properties of an ellipse,

$$a^2 = b^2 + \tfrac{1}{4} d^2 \quad , \qquad 3.1.1$$

and, from Eq. (1),

$$b = \tfrac{1}{2} d \xi_0 \quad . \qquad 3.1.2$$

The radius of curvature of the ellipse at $(r, z) = (0, b)$ (see Figure 2) is given by

$$R = a^2/b = \tfrac{1}{2} d(\xi_0^2 + 1)/\xi_0 \quad . \qquad 3.1.3$$

Thus the specification of the equal radii of curvature R of the laser mirrors and the separation $2b$ of the mirrors defines the parameters ξ_0 and d of the spheroid which matches the laser configuration. Confocal mirror spacing is given by $2b = R$, yielding $d = R$ and $\xi_0 = 1$ for the equivalent spheroid.

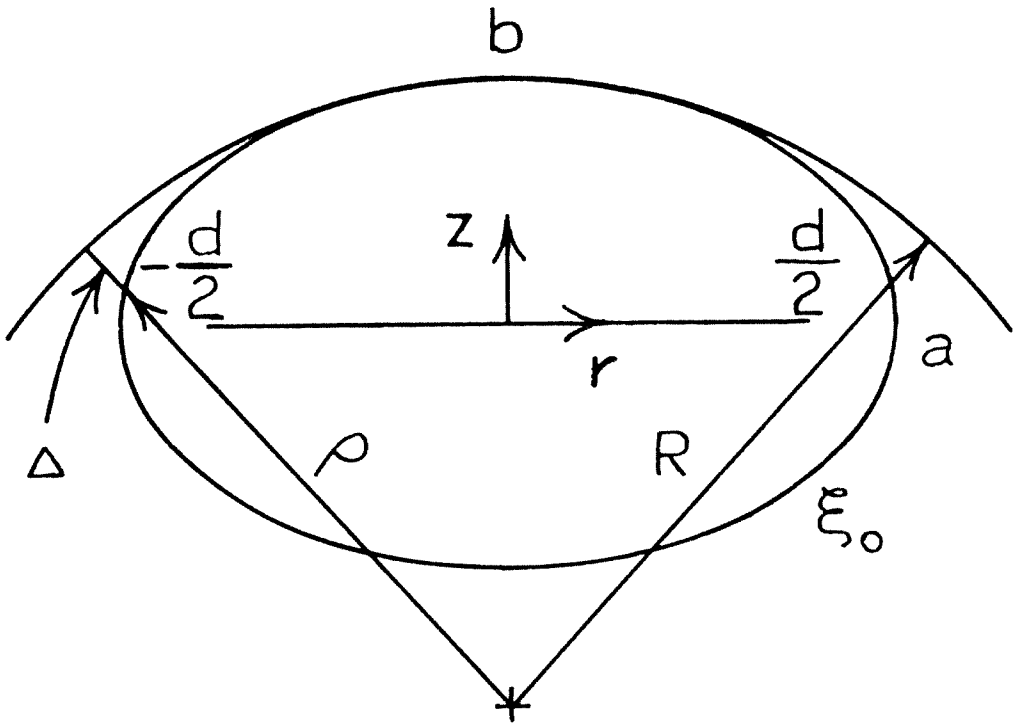

Figure 2. Parameters of an oblate spheroid, and the spherical surface matching its radius of curvature on the rotational axis.

3.2 Two Confocal Spheroidal Surfaces

In the case of a convex-concave mirrors system, the parameters of the equivalent pair of confocal spheroids are given by (see Figure 3)

$$R_1 = a_1^2/b_1 = \tfrac{1}{2}\, d(\xi_1^2 + 1)/\xi_1$$

$$R_2 = a_2^2/b_2 = \tfrac{1}{2}\, d(\xi_2^2 + 1)/\xi_2 \qquad 3.2.1$$

$$b_2 - b_1 = \tfrac{1}{2}\, d(\xi_2 - \xi_1) \quad ,$$

where $b_2 - b_1$ is the mirror separation.

3.3 Criteria for Matching Laser to Spheroid

The deviation of the spheroidal surface from the mirror surface must be small compared to a wavelength in the region of significant field strength. Thus (see Figure 2)

$$\Delta = R - o = (1 - b\rho/a^2)\,(a^2/b) \ll \lambda \qquad 3.3.1$$

places a limit on the laser beam width at the mirror. The equation of the ellipse,

$$(r/a)^2 + (z/b)^2 = 1 \quad , \qquad 3.3.2$$

with the expression for ρ ,

$$\rho^2 = r^2 + [z + (R - b)]^2 \quad , \qquad 3.3.3$$

yields

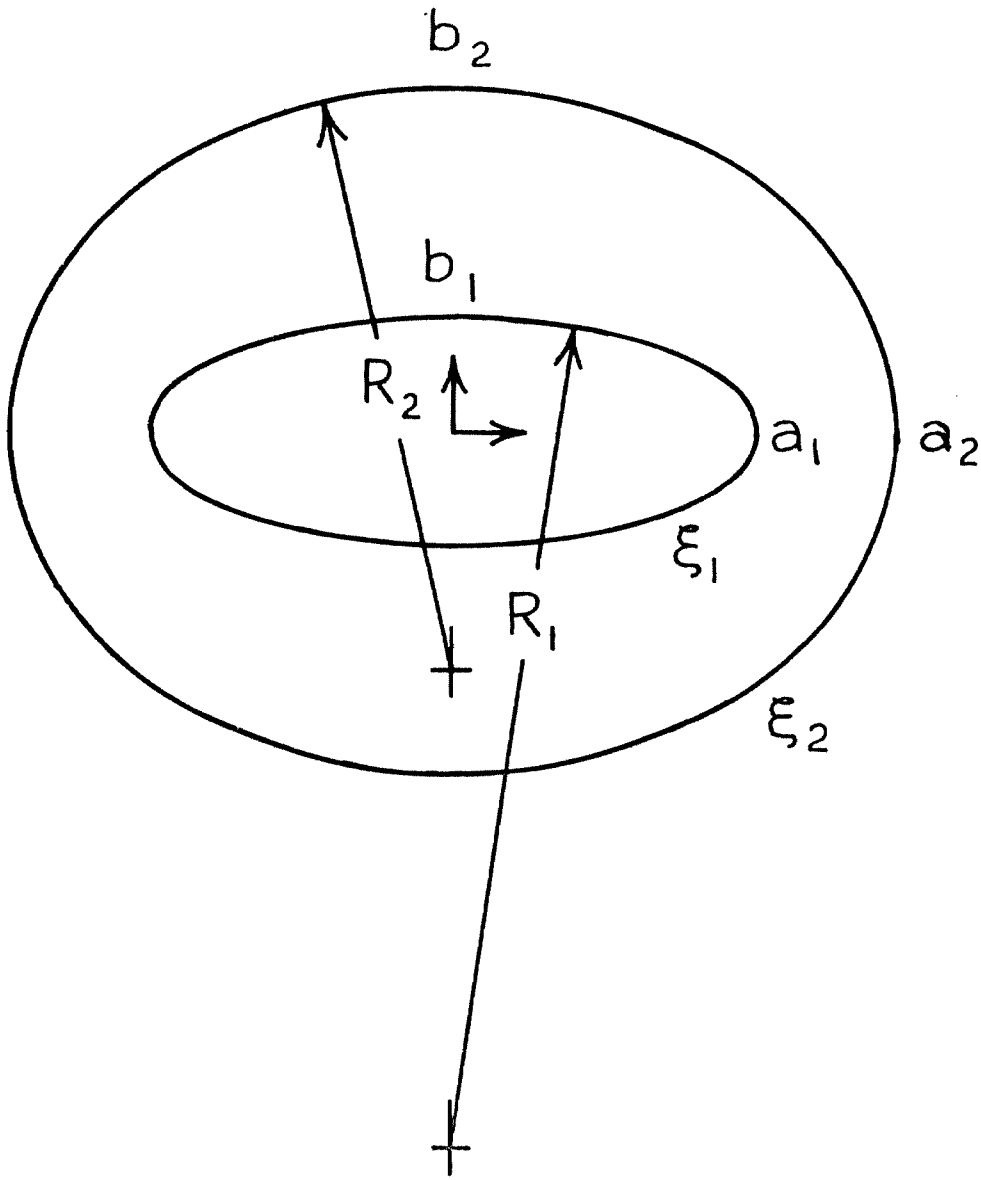

Figure 3. Parameters of a double spheroidal surface cavity, and the radii of curvature of the matching spherical surfaces on the rotational axis.

$$\rho^2 = r^2 + b^2\left(1 - \frac{r^2}{a^2}\right) + 2(a^2 - b^2)\left(1 - \frac{r^2}{a^2}\right)^{\frac{1}{2}} + \left(\frac{a^2 - b^2}{b}\right)^2 \quad . \quad 3.3.4$$

Since $r^2 < a^2$ is clearly required, the square root can be expanded. Collecting terms gives

$$\frac{b\rho}{a^2} = \left[1 - \frac{b^2}{a^2}\left(1 - \frac{b^2}{a^2}\right)\left(\frac{1}{4}\frac{r^4}{a^4} + \frac{1}{8}\frac{r^6}{a^6} + \ldots\right)\right]^{\frac{1}{2}} \quad . \quad 3.3.5$$

For a typical laser, $a^2 \gg b\lambda$. Then, from Eq. 3.3.1, $b\rho/a^2$ must be close to one; and the terms in r^2/a^2 in Eq. 3.3.5 must be small compared to one. Expansion and insertion into Eq. 3.3.1 yields

$$\frac{a^2}{b\lambda}\left[\frac{1}{2}\frac{b^2}{a^2}\left(1 - \frac{b^2}{a^2}\right)\left(\frac{1}{4}\frac{r^4}{a^4} + \frac{1}{8}\frac{r^6}{a^6} + \ldots\right)\right] \ll 1 \quad . \quad 3.3.6$$

If $r^2 \ll 2a^2$, then all but the lowest order term in r^2/a^2 may be dropped, yielding, in terms of the parameters of both the ellipse and the spheroid,

$$\frac{1}{8}\frac{b}{\lambda}\left(1 - \frac{b^2}{a^2}\right)\frac{r^4}{a^4} = \frac{\xi_0}{(\xi_0^2 + 1)^3}\frac{r^4}{d^3\lambda} \ll 1 \quad . \quad 3.3.7$$

A typical laser is the one meter spacing, one meter radius confocal mirrors laser. If a wavelength of $2\pi \times 10^{-7}$ meters (in the visible) is assumed, the parameters for this configuration are

$$a = \tfrac{1}{2}\sqrt{2}\ m$$

$$b = \tfrac{1}{2}\ m$$

$$d = 1\ m$$

$$\xi_0 = 1 \qquad 3.3.8$$

$$R = 1\ m$$

$$\lambda = 2\pi \times 10^{-7}\ m$$

$$k = 2\pi/\lambda = 10^{7}\ m^{-1}$$

$$c = \tfrac{1}{2}\ kd = 5 \times 10^{6}$$

where c will be defined later. With these numbers, the left hand side of Eq. 3.3.7 is less than 10^{-2} if r is less than 1.5 centimeters. This value of r yields a value for $\frac{1}{2}\ r^2/a^2$ of 2.25×10^{-4}, verifying the approximation made in deriving Eq. 3.3.7. Thus a spheroidal surface is an excellent approximation to a laser mirror for usual laser beam widths.

3.4 Comparison with Previously Derived Criteria

The analysis of Boyd and Gordon (7) involves the use of three conditions (given here in their notation) on the physical system parameters: from the argument of the exponential factor,

$$a^2/b\lambda \ll 1 \ll b^2/a^2\ , \qquad 3.4.1$$

from the $1/r$ factor,

$$a^2/b^2 \ll \frac{1}{4} \quad , \qquad 3.4.2$$

and from $|ik| \gg \frac{1}{r}$,

$$\lambda/d \ll 2\pi \quad . \qquad 3.4.3$$

These conditions are parallel to the conditions derived in this section for $\xi_0 = 1$ (given in the notation of this paper, but written so that there is a one to one correspondence between quantities in the expressions),

$$r^2/(2b)\lambda \ll 8\,(2b)^2/r^2 \quad , \qquad 3.4.4$$

and

$$r^2/(2b)^2 \ll 1 \quad . \qquad 3.4.5$$

For the case of light wavelengths much less than cavity dimensions, c is much greater than one: yielding

$$\lambda/(2b) \ll \pi \quad . \qquad 3.4.6$$

Thus the same requirements on the physical system are expressed in the similar conditions on the system parameters.

CHAPTER FOUR

WAVE EQUATION AND BOUNDARY CONDITIONS

Assumption of the forms

$$\bar{E}(\bar{r},t) = \bar{E}(\bar{r})\, e^{j\omega t}$$
$$\bar{H}(\bar{r},t) = \bar{H}(\bar{r})\, e^{j\omega t} \qquad 4.1$$

for the electromagnetic field vectors in a source-free, non-conducting scalar medium reduces Maxwell's equations to (see Appendix A)

$$\bar{\nabla} \times \bar{\nabla} \times \bar{E}(\bar{r}) - k^2 \bar{E}(\bar{r}) = 0$$
$$\bar{\nabla} \times \bar{\nabla} \times \bar{H}(\bar{r}) - k^2 \bar{H}(\bar{r}) = 0 \qquad 4.2$$

or, equivalently,

$$\nabla^2 \bar{E}(\bar{r}) + k^2 \bar{E}(\bar{r}) = 0$$
$$\nabla^2 \bar{H}(\bar{r}) + k^2 \bar{E}(\bar{r}) = 0 \qquad 4.3$$

where $k^2 = \omega^2 \mu\varepsilon$. The boundary conditions are

$$\bar{n} \times \bar{E} = 0$$
$$\bar{n} \cdot \bar{H} = 0 \qquad 4.4$$

on the cavity boundary surfaces, where $\bar{n}$ is the unit vector normal to the boundary surface: for the spheroidal cavities of interest, $\bar{n} = \bar{e}_\xi$. The single surface cavity will be specified by $\xi = \xi_o$;

the double surface cavity will be specified by $\xi = \xi_1$ and $\xi = \xi_2$, with $\xi_1 < \xi_2$.

CHAPTER FIVE

ASYMPTOTIC FORM OF SCALAR WAVE FUNCTION

5.1 Solutions of Scalar Wave Equation

The solutions of the vector wave equation are given in terms of the solutions ψ of the scalar wave equation (see Appendix C, Eq. C.5 and C.6)

$$\nabla^2 \psi + k^2 \psi = 0 \, . \qquad 5.1.1$$

The solutions of this equation in spheroidal coordinates have been given in several notations (31-37). In this paper the forms of the solutions and their notations are those of Flammer (31).

A general solution ψ suitable for use in the cavity configurations of interest can be written as a linear combination of the functions (see Appendix C, Eq. C.9 and C.10)

$$\psi e_{mn}^{(i)}(-jc,\eta,j\xi) = S_{mn}(-jc,\eta)\, R_{mn}^{(i)}(-jc,j\xi) \cos m\varphi \qquad 5.1.2$$

and $\psi o_{mn}^{(i)}(-jc,\eta,i\xi)$, the same except for $\sin m\varphi$ vice $\cos m\varphi$, where $S_{mn}(-jc,\eta)$ is the angular function finite at $z = \pm 1$, and $R_{mn}^{(1)}(-jc,j\xi)$ and $R_{mn}^{(2)}(-jc,j\xi)$ are the standing wave forms of the radial function. The function $R_{mn}^{(2)}$ must be excluded, for reasons of continuity of ψ and its normal derivative, when the surface $\xi = 0$ is included in the cavity. The indices m and n are zero or positive integers, with $n \geq m$. The number $c = \frac{1}{2} kd$ is a dimensionless parameter of Eq. 5.1.1 in its explicit form for spheroidal

coordinates. Since $c \gg 1$ is valid for usual lasers, the forms of the functions useful for large c are of particular interest.

5.2 Asymptotic Form of Oblate Spheroidal Angular Wave Function

Flammer (31) gives the asymptotic form of the oblate spheroidal angular function:

$$S_{mn}(-jc, \eta \approx \pm 1) \sim (\pm 1)^{n-m} \, c^{\frac{1}{2}m} (1 - \eta^2)^{\frac{1}{2}m} \, e^{-c(1 \mp \eta)} \, L_\nu^m[2c(1 \mp \eta)] \qquad 5.2.1$$

where $L_n^m(x)$ is the associated Laguerre polynomial of the first kind (38-40), and

$$\begin{aligned} \nu &= \tfrac{1}{2}(n - m) \quad , \qquad (n - m) \text{ even} \\ &= \tfrac{1}{2}(n - m - 1) \quad , \qquad (n - m) \text{ odd} \quad . \end{aligned} \qquad 5.2.2$$

Using the scale factor h_φ and defining the quantity

$$\begin{aligned} r_o &= \tfrac{1}{2} d(\xi^2 + 1)^{\frac{1}{2}} \quad \text{gives} \\ \eta &= \pm \left[1 - (r/r_o)^2\right]^{\frac{1}{2}} \quad , \end{aligned} \qquad 5.2.3$$

where r is the cylindrical radius to a point (η, ξ). For the laser configuration described by the numbers of Eq. 3.3.8, r_o has a minimum value of 0.5 meter. Since the restriction has been made that the significant field strength is contained within $r = 0.015$ meter, it is

clear that $(r/r_o)^2 \ll 1$, permitting the expansion of the square root in Eq. 5.2.3. Using the plus sign, for $\eta \approx 1$, yields, to first order in $(r/r_o)^2$,

$$1 - \eta \approx 1 - \left[1 - \tfrac{1}{2}(r/r_o)^2\right]^{\frac{1}{2}} \approx \tfrac{1}{2}(r/r_o)^2 \quad . \qquad 5.2.4$$

Thus the angular function can be written in terms of r and ξ in the form

$$S_{mn}(-jc, \eta \approx \pm 1) \sim (\pm 1)^{n-m}\, \alpha^{\frac{1}{2}m}\, e^{-\frac{1}{2}\alpha}\, L_\nu^m(\alpha) \quad , \qquad 5.2.5$$

where $\alpha = c(r/r_o)^2$. This function has even and odd symmetry about $\xi = 0$ with $(n - m)$ even and odd, for the same value of ν .

5.3 Asymptotic Form of Oblate Spheroidal Radial Wave Function

An exact form of the oblate spheroidal radial function useful for large c is given by Flammer (31):

$$R_{mn}^{(1)},\ jR_{mn}^{(2)} = (\xi^2 + 1)^{\frac{1}{2}m}\, j^{-(n-m+1)} \sum_{s=-\nu}^{\infty} A_s^{mn}$$

$$\left\{ e^{-jc\xi}\, U_{\nu+s}^m[2c(1 + j\xi)] \pm (-1)^{n-m+1}\, e^{jc\xi}\, U_{\nu+s}^m[2c(1 - j\xi)] \right\}$$

5.3.1

where $U_n^m(x)$ is the associated Laguerre polynomial of the second kind (38) and A_s^{mn} is given by

$$A_s^{mn} = A_o^{mn} \sum_{k=|s|}^{\infty} a_k^{\,s}(m,n)\, c^{-k} \quad . \qquad 5.3.2$$

Flammer has tables of $a_k^{\,s}(m,n)$, polynomials in m and n , for $k, |s| = 1,2,3,4$. The asymptotic development for $U_n^{\,m}(x)$ when $|x| \gg 1$ is (38)

$$U_n^{\,m}(x) \sim \pi^{-1}\, e^{\pm j(n+\frac{1}{2})\pi}(m+n)!\; x^{-(n+m+1)}\, e^{x} \quad , \qquad 5.3.3$$

where the upper sign is used when $0 < \arg x < \pi$, and the lower sign is used when $-\pi < \arg x < 0$. Inserting A_s^{mn} and $U_{\nu+s}^{m}$ into Eq. 5.3.1 yields, after some manipulation,

$$R_{mn}^{(1),(2)} \sim \sum_{s=-\nu}^{\infty} \frac{(\nu+s+m)!}{2^s(\xi^2+1)^{\frac{1}{2}(\nu+s+1)}} \begin{Bmatrix} \cos \\ \sin \end{Bmatrix} \theta \sum_{k=|s|}^{\infty} a_k^{\,s}(m,n)\, c^{-(k+s+1)} \quad , \qquad 5.3.4$$

where

$$\theta = c\xi + (2\nu + 2s + m - n)\frac{\pi}{2} - (m + \nu - s + 1)\,\mathrm{Tan}^{-1}\,\xi \quad . \qquad 5.3.5$$

The dominant terms in this double sum are those of lowest $k + s$. These are the $\nu + 1$ terms for which $k = -s = \nu\,,\ \nu - 1,\ \ldots\,,1,0$. Dropping higher order terms yields

$$R_{mn}^{(1),(2)} \sim c^{-1} \sum_{s=c}^{\nu} 2^s(\nu - s + m)!\; (\xi^2+1)^{-\frac{1}{2}(\nu-s+1)} \begin{Bmatrix} \cos \\ \sin \end{Bmatrix} \theta'\; a_s^{\,-s}(m,n) \quad , \qquad 5.3.6$$

where $\theta'(s) = \theta(-s)$. These functions are valid for large values of c and all values of ξ . In the limit of large values of ξ , the sum is dominated by the term $s = \nu$, yielding the normalization satisfied by the exact radial functions:

$$R_{mn}^{(1)} \sim \text{const } (c\xi)^{-1} \cos\left[c\xi - (n+1)\frac{\pi}{2}\right] \qquad 5.3.7$$

and similarly with $\sin[\,]$ for $R_{mn}^{(2)}$.

CHAPTER SIX

VECTOR WAVE FUNCTION SOLUTION

6.1 General Solutions

Soleroidal solutions of the vector wave equation

$$\bar{\nabla} \times (\bar{\nabla} \times \bar{A}) - k^2 \bar{A} = 0 \qquad 6.1.1$$

can be written in the forms (see Appendix B)

$$\bar{A}_1 = \bar{\nabla} \psi \times \bar{a}$$

$$\bar{A}_2 = k^{-1} \bar{\nabla} \times (\bar{\nabla} \times \bar{a} \varphi) \qquad 6.1.2$$

where $\bar{a}$ is a constant vector or the radius vector and ψ, φ are the scalar wave functions of Eq. 5.1.2.

If the electromagnetic field vectors are derived from $\bar{A}_1$ by the equations

$$\bar{E}_1 = -j\omega\bar{A}_1$$

$$\bar{H}_1 = \mu^{-1} \nabla \times \bar{A}_1 \qquad 6.1.3$$

and $\bar{a} = \bar{e}_x$ is chosen, then $\bar{E}$ and $\bar{H}$ are given by

$$(Ee_{mn}^{x(i)})_{\eta,\xi,\varphi} = -j\omega(Me_{mn}^{x(i)})_{\eta,\xi,\varphi}$$

$$(He_{mn}^{x(i)})_{\eta,\xi,\varphi} = k\mu^{-1} (Ne_{mn}^{x(i)})_{\eta,\xi,\varphi} \qquad 6.1.4$$

and similarly for $e \rightarrow o$, where the functions on the right hand side

are straightforward but lengthy expressions calculated from Eq. 6.1.2 and tabulated by Flammer (31), involving S_{mn}, R_{mn}, their first and second derivatives, and trigonometric functions of $m\varphi$. Examination of these functions shows, as is well known, that they will not permit the boundary conditions to be exactly matched.

6.2 Asymptotic Form of Solutions

For the spheroidal cavities of interest, however, with large values of c and $\eta \approx \pm 1$, use can be made of

$$1 - \eta^2 = (1 + \eta)(1 - \eta) \approx 2(1 \mp \eta)$$

$$\xi^2 + \eta^2 \approx \xi^2 + 1 \qquad 6.2.1$$

$$dR^{(i)}/d\xi \approx (-1)^i \, cR^{(j)} \; ; \quad i,j = 1,2 \text{ or } 2,1$$

to reduce the functions to the terms of highest order in c, giving (the indices of Eq. 6.1.4 are omitted for clarity)

$$E_\eta \approx jc \, S_{mn}(-1)^i \, R_{mn}^{(j)} \sin\varphi \cos m\varphi$$

$$E_\xi \approx -j \left[\frac{2(1 \mp \eta)}{\xi^2 + 1}\right]^{\frac{1}{2}} R_{mn}^{(i)} \left[\frac{d}{d\eta} S_{mn} \sin\varphi \cos m\varphi \right.$$

$$\left. + \frac{m}{2(1 \mp \eta)} S_{mn} \cos\varphi \sin m\varphi\right]$$

$$E_\varphi \approx -jc \, S_{mn}(-1)^i \, R_{mn}^{(j)} \cos\varphi \cos m\varphi$$

6.2.2

$$H_\eta \approx -c \left(\frac{\epsilon}{\mu}\right)^{\frac{1}{2}} S_{mn} R_{mn}^{(i)} \cos\varphi \cos m\varphi$$

$$H_\xi \approx -\left(\frac{\epsilon}{\mu}\right)^{\frac{1}{2}} \left[\frac{2(1 \mp \eta)}{\xi^2 + 1}\right]^{\frac{1}{2}} (-1)^i R_{mn}^{(j)} \left[\frac{d}{d\eta} S_{mn} \cos\varphi \cos m\varphi - \frac{m}{2(1 \mp \eta)} \sin\varphi \sin m\varphi\right]$$

$$H_\varphi \approx -c \left(\frac{\epsilon}{\mu}\right)^{\frac{1}{2}} S_{mn} R_{mn}^{(i)} \sin\varphi \cos m\varphi \quad .$$

6.2.3

6.3 Nature of Solutions

Eo and Ho are given by the same expressions with $\cos m\varphi \rightarrow \sin m\varphi$ and $\sin m\varphi \rightarrow -\cos m\varphi$. E has only y and/or z components; and, since the ξ components of E and H are smaller by a factor of c^{-1} from the others and the η and φ components are suitably related, it is clear that this mode is approximately a plane wave, with $\overline{E} \approx \overline{e}_y E_y$ and $\overline{H} \approx \overline{e}_x H_x$. A choice of $\overline{a} = \overline{e}_y$ gives $\overline{E} \approx \overline{e}_x E_x$ and $\overline{H} \approx \overline{e}_y H_y$; $\overline{a} = \overline{e}_z$ or $\overline{r}$ gives $\overline{E} \approx \overline{e}_\varphi E_\varphi$.

The approximately transverse modes of Eq. 6.2.2 and 6.2.3 are characterized by linear polarization, m nodal lines in the φ direction, and ν nodal lines in the r direction. Even and odd $(n - m)$ for the same ν gives the modes even or odd symmetry about $\xi = 0$. These modes have been photographed by Rigrod (41). The circular mirrors section of Figure 18 of Fox and Li (4) illustrate additional

modes of Eq. 6.2.2 and 6.2.3.

If the electromagnetic field vectors are derived from $\overline{A}_2$, the results are simply related to the fields we have already found:

$$\overline{E}_2 = -j\omega\overline{A}_2 = -j\omega k^{-1}\,\overline{\nabla} \times \overline{A}_2 = -j(\mu/\epsilon)^{\frac{1}{2}}\,\overline{H}_1$$

$$\overline{H}_2 = \mu^{-1}\,\overline{\nabla} \times \overline{A}_2 = (k\mu)^{-1}\,\overline{\nabla} \times (\overline{\nabla} \times \overline{A}_1) = k\mu^{-1}\,\overline{A}_1 = j(\epsilon/\mu)^{\frac{1}{2}}\,\overline{E}_1 \,. \qquad 6.3.1$$

6.4 Matching Boundary Conditions

The approximate electromagnetic field vectors given by Eq. 6.2.2, 6.2.3 and 6.3.1 are suited to matching the boundary conditions in the cavities of interest. For the field vectors derived from $\overline{A}_1$, within the single surface cavity,

$$R_{mn}^{(i)} \rightarrow R_{mn}^{(1)}$$

$$(-1)^i\, R_{mn}^{(j)} \rightarrow -R_{mn}^{(2)} \,, \qquad 6.4.1$$

and the boundary conditions are satisfied if c takes on any of the values c_{mnq}, $q = 1,2, \ldots, \infty$, satisfying

$$R_{mn}^{(2)}\,(-jc_{mnq}\,,\ j\xi_0) = 0 \,. \qquad 6.4.2$$

Within the double surface cavity,

$$R_{mn}^{(i)} \rightarrow -R_{mn}^{(1)}(-jc,\ j\xi_1)\ R_{mn}^{(1)}(-jc,\ j\xi) - R_{mn}^{(2)}(-jc,\ j\xi)\ R_{mn}^{(2)}(-jc,\ j\xi_1)$$

$$(-1)^i\ R_{mn}^{(j)} \rightarrow R_{mn}^{(1)}(-jc,\ j\xi_1)\ R_{mn}^{(2)}(-jc,\ j\xi) - R_{mn}^{(1)}(-jc,\ j\xi)\ R_{mn}^{(2)}(-jc, j\xi_1)$$

6.4.3

and c is determined by

$$R_{mn}^{(1)}(-jc_{mnq},\ j\xi_1)\ R_{mn}^{(2)}(-jc_{mnq},\ j\xi_2) - R_{mn}^{(1)}(-jc_{mnq},\ j\xi_2) R_{mn}^{(2)}(-jc_{mnq}, j\xi_1) = 0$$

6.4.4

For the field vectors derived from $\bar{A}_2$, within the single surface cavity, Eq. 6.4.1 holds, and c is given by

$$R_{mn}^{(1)}(-jc_{mnq},\ j\xi_0) = 0 \quad . \tag{6.4.5}$$

Within the double surface cavity,

$$R_{mn}^{(i)} \rightarrow R_{mn}^{(1)}(-jc,\ j\xi_1)\ R_{mn}^{(2)}(-jc,\ j\xi) - R_{mn}^{(1)}(-jc,\ j\xi)\ R_{mn}^{(2)}(-jc,\ j\xi_1)$$

$$(-1)^i\ R_{mn}^{(j)} \rightarrow R_{mn}^{(1)}(-jc,\ j\xi_1)\ R_{mn}^{(1)}(-jc,\ j\xi) + R_{mn}^{(2)}(-jc, j\xi)\ R_{mn}^{(2)}(-jc,\ j\xi_1)$$

6.4.6

and c is determined by Eq. 6.4.4.

CHAPTER SEVEN

ROTATIONALLY SYMMETRIC SOLUTIONS

7.1 Form of Solutions

It is well known (42-50) that boundary conditions can be matched exactly on a spheroid by restricting the fields to rotational symmetry: either a transverse electric vector (TE) set with $\overline{E} \equiv \overline{e}_{\varphi} E_{\varphi}(\eta,\xi)$, or a transverse magnetic vector (TM) set with $\overline{H} \equiv \overline{e}_{\varphi} H_{\varphi}(\eta,\xi)$. Upon writing $\Phi(\eta,\xi)$ for the φ component of either set, reducing the vector wave equation to a scalar equation for this component, and comparing this equation with the scalar wave equation (see Appendix C), it becomes clear that Φ can be written as a linear superposition of the components of the orthogonal set Φ_n , complete only for rotationally symmetric functions, given by

$$\Phi_n^{(i)}(-jc,\ \eta,\ j\xi) = S_{1n}(-jc,\ \eta)\ R_{1n}^{(i)}(-jc,\ j\xi) \quad . \qquad 7.1.1$$

The other components of the electromagnetic field vectors are given by

$$\begin{aligned}
H_{\eta} &= -(j\omega\mu h_{\xi} h_{\varphi})^{-1} \left[\partial(h_{\varphi} E_{\varphi})/\partial\xi\right] \\
H_{\xi} &= (j\omega\mu h_{\eta} h_{\varphi})^{-1} \left[\partial(h_{\varphi} E_{\varphi})/\partial\eta\right] \\
E_{\eta} &= (j\omega\varepsilon h_{\xi} h_{\varphi})^{-1} \left[\partial(h_{\varphi} H_{\varphi})/\partial\xi\right] \\
E_{\xi} &= -(j\omega\varepsilon h_{\eta} h_{\varphi})^{-1} \left[\partial(h_{\varphi} H_{\varphi})/\partial\eta\right] \quad .
\end{aligned} \qquad 7.1.2$$

7.2 Matching Boundary Conditions

The TE set will satisfy the boundary conditions within a single surface cavity if the radial part of E_φ has the form $R_{ln}^{(1)}(-jc, j\xi)$ and c takes on any of the values c_{nq} satisfying the equation

$$R_{ln}^{(1)}(-jc_{nq}, j\xi_0) = 0 \quad . \tag{7.2.1}$$

Within a double surface cavity the radial part has the form

$$R_{ln}^{(1)}(-jc, j\xi_1)\, R_{ln}^{(2)}(-jc, j\xi) - R_{ln}^{(1)}(-jc, j\xi)\, R_{ln}^{(2)}(-jc, j\xi_1)$$

and c_{nq} is given by

$$R_{ln}^{(1)}(-jc_{nq}, j\xi_1)\, R_{ln}^{(2)}(-jc_{nq}, j\xi_2) - R_{ln}^{(1)}(-jc_{nq}, j\xi_2)\, R_{ln}^{(2)}(-jc_{nq}, j\xi_1) = 0. \tag{7.2.2}$$

The TM set will satisfy the boundary conditions within the single surface cavity if the radial part of H_φ has the form $R_{ln}^{(1)}(-jc, j\xi)$ and c is given by

$$\left[\partial(h_\varphi H_\varphi)/\partial\xi\right]_{\xi=\xi_0} = 0 \quad , \tag{7.2.3}$$

which becomes

$$\xi_0(\xi_0^2 + 1)^{-\frac{1}{2}}\, R_{ln}^{(1)}(-jc_{nq}, j\xi_0) + (\xi_0^2 + 1)^{\frac{1}{2}} \left[d(R_{ln}^{(1)})/d\xi\right]_{\xi=\xi_0} = 0 \quad . \tag{7.2.4}$$

Within the double surface cavity the radial part has the form $A^{(1)} R_{ln}^{(1)}(-jc, j\xi) - A^{(2)} R_{ln}^{(2)}(-jc, j\xi)$ where, from consideration of Eq. 7.2.3 and 7.2.4,

$$A^{(1)}(-jc, j\xi_1) = \xi_1(\xi_1^2+1)^{-\frac{1}{2}} R_{ln}^{(2)}(-jc, j\xi_1) + (\xi_1^2+1)^{\frac{1}{2}} \left[d(R_{ln}^{(2)})/d\xi \right]_{\xi=\xi_1} \qquad 7.2.5$$

and similarly for $(1) \rightarrow (2)$, $(2) \rightarrow (1)$. The values of c_{nq} are determined from the equation

$$A^{(1)}(-jc_{nq}, j\xi_1)\, A^{(2)}(-jc_{nq}, j\xi_2) - A^{(2)}(-jc_{nq}, j\xi_1)\, A^{(1)}(-jc_{nq}, j\xi_2) = 0 \; . \qquad 7.2.6$$

7.3 Nature of Solutions

A single mode of oscillation is specified by the two quantities n and q . The quantity $(n - 1)$ is the number of nodes in the radial direction and q is associated with the number of nodes in the ξ direction. For the single surface cavity, n and q are coupled by the requirement of a continuous field gradient about the surface $\xi = 0$. The frequency of oscillation for a given mode is given by

$$\omega = 2\, cd^{-1}\, (\mu\epsilon)^{-\frac{1}{2}} \; . \qquad 7.3.1$$

The TE_{nq} mode in a single surface cavity, for example, is given by

$$\overline{E}_{nq}(\eta, \xi, t) = \overline{e}_{\varphi}\, E_0\, S_{ln}(-jc_{nq}, \eta)\, R_{ln}^{(1)}(-jc_{nq}, j\xi)\, e^{j\omega_{nq} t} \qquad 7.3.2$$

where c_{nq} is given by Eq. 7.2.1, ω_{nq} by Eq. 7.3.1, and the magnetic vector by Eq. 7.1.2.

The expressions written in this section are exact. If the forms of these expressions for large c are considered, then Eq. 7.2.1, 7.2.2, 7.2.4 and 7.2.6 become identical to Eq. 6.4.5, 6.4.4, 6.4.2, and 6.4.4.

CHAPTER EIGHT

EIGENVALUE DETERMINATION FOR SIMPLE MODES

When $\nu = 0$, the expressions for the radial functions in Eq. 5.3.4 reduce to a single term,

$$R^{(1)}_{\nu=0} = c^{-1}(\xi^2 + 1)^{-\frac{1}{2}} \cos \theta_{mn} \qquad 8.1$$

and $\cos \rightarrow \sin$ for $(1) \rightarrow (2)$, where

$$\theta_{mn}(\xi) = c\xi - \tfrac{1}{2}\pi(n - m) - (m + 1)\,\mathrm{Tan}^{-1}\,\xi \quad . \qquad 8.2$$

The eigenvalue equations, (a) Eq. 6.4.5, for the $\bar{A}_2$ or TE modes in the single surface cavity, (b) Eq. 6.4.2, for the $\bar{A}_1$ or TM modes in the single surface cavity, and (c) Eq. 6.4.4, for the $\bar{A}_1$ or $\bar{A}_2$, TE or TM modes in the double surface cavity, then become

$$\begin{aligned} &(a) \quad \cos \theta_{mnq}(\xi_0) = 0 \\ &(b) \quad \sin \theta_{mnq}(\xi_0) = 0 \\ &(c) \quad \sin\left[\theta_{mnq}(\xi_2) - \theta_{mnq}(\xi_1)\right] = 0 \end{aligned} \qquad 8.3$$

which are satisfied by setting

$$\begin{aligned} &(a) \quad \theta_{mnq}(\xi_0) = (q - \tfrac{1}{2})\pi \\ &(b) \quad \theta_{mnq}(\xi_0) = q\pi \\ &(c) \quad \theta_{mnq}(\xi_2) - \theta_{mnq}(\xi_1) = q\pi \quad , \end{aligned} \qquad 8.4$$

where $q = 1,2, \ldots, \infty$, yielding

$$\text{(a)} \quad c_{mnq}\,\xi_0 = \tfrac{1}{2}\pi\,(2q + n - m - 1) + (m + 1)\,\mathrm{Tan}^{-1}\,\xi_0$$

$$\text{(b)} \quad c_{mnq}\,\xi_0 = \tfrac{1}{2}\pi\,(2q + n - m) + (m + 1)\,\mathrm{Tan}^{-1}\,\xi_0$$

$$\text{(c)} \quad c_{mnq}\,(\xi_2 - \xi_1) = q\pi + (m + 1)(\mathrm{Tan}^{-1}\,\xi_2 - \mathrm{Tan}^{-1}\,\xi_1) \quad . \qquad 8.5$$

The number of half cavity wavelengths N_{mnq} is given by

$$\text{(a), (b)} \quad \pi N_{mnq} = 2\left[\theta_{mnq}\,(\xi_0) - \theta_{mnq}\,(0)\right]$$

$$\text{(c)} \qquad \pi N_{mnq} = \theta_{mnq}\,(\xi_2) - \theta_{mnq}\,(\xi_1) \quad , \qquad 8.6$$

yielding

$$\text{(a)} \quad N_{mnq} = 2q + n - m - 1$$

$$\text{(b)} \quad N_{mnq} = 2q + n - m \qquad 8.7$$

$$\text{(c)} \quad N_{mnq} = q \quad .$$

CHAPTER NINE

DISCUSSION OF RESULTS

9.1 General

The approach to the laser mode problem taken in this paper differs from the more familiar approaches (4,7-12,15-23,51) in that in this paper the resonator has been assumed to be a perfect cavity, permitting a vector solution for the electromagnetic fields, rather than retaining a more realistic resonator configuration, and finding a scalar solution for the fields.

The two approaches complement one another. For example, the vector solution shows that the magnitude of the longitudinal field component is c^{-1} smaller than the magnitudes of the transverse components, indicating that the scalar solution is good to within c^{-1}, a very good accuracy. The perfectly conducting closed surface boundary and lossless dielectric form a lossless cavity, and so diffraction loss consideration is not possible. The low-loss configurations of Yariv and Gordon (52) are reproduced in part by the oblate spheroidal cavities considered. It becomes clear that, as stated by Zimmerer (29), surfaces of constant phase are oblate spheroids and that the lines of propagation lie along hyperboloids, agreeing, within the region of approximation of spherical surfaces by spheroids, with the analytical results of Boyd and Gordon (7) and the numerical results of Fox and Li (4).

The factor $\exp\left(-\frac{1}{2} cr^2/r_o^2\right)$ clarifies the assumptions on

which the analysis of this paper is based. The requirement that the field strength be small at the edge of the mirror yields

$$ca^2/2r_o^2 \gg 1 \qquad 9.1.1$$

where a is the radius of the mirror. This can be written in terms of a mixture of the spheroidal parameters d and ξ_o and the laser parameters d', the mirror separation, and R, the mirror radius:

$$\frac{.61\pi}{1+\xi_o^2}\frac{a}{2d} = \frac{.61\pi}{4}\frac{a}{d'}\frac{d}{R} \gg .61\frac{\lambda}{a}\ , \qquad 9.1.2$$

which requires that the half cone angle subtended at one mirror center by the other, multiplied by a geometrical configuration ratio d/R measuring the degree of closeness to confocal configuration, must be much greater than the half cone angle subtended by the Airy disk of the diffraction of a plane wave from a circular aperture of the same area as the mirror. As the configuration approaches spherical spacing, d' approaches $2R$ and d approaches zero. As the configuration approaches plane-parallel spacing, d approaches infinity and ξ_o approaches zero. Thus the analysis is not valid for these limiting cases.

9.2 Correlation with Confocal Resonator Analysis

Boyd and Gordon (7) give an expression for the linearly polarized traveling wave field in a confocal resonator which is valid when the mirror area $4a^2$ is much larger than $4b\lambda$, where b is

the mirror separation. From it the linearly polarized standing wave field can be determined to be

$$E_{mn}(x,y,z) = \beta\, H_m(\beta X)\, H_n(\beta Y) \exp\left(-kw^2\beta^2/2b\right) \cdot$$

$$\cdot \cos\left[\tfrac{1}{2} kb\bar{\xi}\left(1 + w^2\beta^2/2b^2\right) - \tfrac{1}{4}\pi\,(1 + m + n)\,\mathrm{Tan}^{-1}\,\bar{\xi}\right] \qquad 9.2.1$$

for the mode even about $z = 0$, and $\cos \rightarrow \sin$ for the mode odd about $z = 0$, where

$$\begin{aligned} \beta &= 2\left(1 + \bar{\xi}^2\right)^{-\frac{1}{2}} \\ X &= x\,(k/b)^{\frac{1}{2}} \\ Y &= y\,(k/b)^{\frac{1}{2}} \\ w^2 &= x^2 + y^2 \\ \bar{\xi} &= 2z/b\,, \end{aligned} \qquad 9.2.2$$

and $H_m(x)$ is the Hermite polynomial (38,39).

It can be shown that the oblate spheroidal surface defined by the parameters $d = b$ and z_o (see Fig. 4) is given by

$$(z/z_o)^2 = 1 - (2w/c)^2/\left[1 + (2z_o/d)^2\right] \qquad 9.2.3$$

and is also defined by the spheroidal parameters d and $\xi = 2z_o/d$. Since $(2w/c)^2 \ll 1$, Eq. 9.2.3 becomes

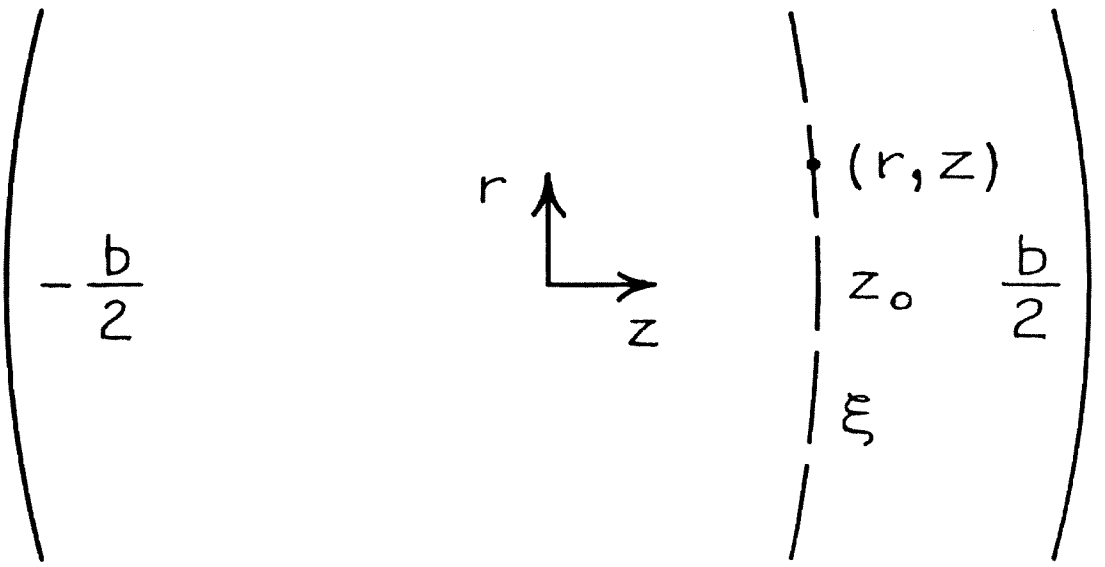

Figure 4. Surface of constant phase (dotted line) in a confocal mirrors laser.

$$z \approx z_o - (2z_o/d)\ (w^2/d)/\left[1 + (2z_o/d)^2\right] \quad , \qquad 9.2.4$$

which is the expression found by Boyd and Gordon (7) for the surface of constant phase intersecting the axis at z_o . It can be written

$$\bar{\xi} \approx \xi \left[1 - (2w^2/d^2)/(1 + \xi^2)\right] \quad . \qquad 9.2.5$$

The approximation $\bar{\xi} \approx \xi$ yields

$$\begin{aligned} 1 + \bar{\xi}^2 &\approx 1 + \xi^2 \\ \mathrm{Tan}^{-1}\,\bar{\xi} &\approx \mathrm{Tan}^{-1}\,\xi \quad , \end{aligned} \qquad 9.2.6$$

and the approximation $\xi \approx \bar{\xi}\left[1 + (2w^2/d^2)/(1 + \bar{\xi}^2)\right]$ yields

$$\bar{\xi}\left[\tfrac{1}{2}b + (w^2/b)\ (1 + \bar{\xi}^2)^{-\frac{1}{2}}\right] \approx \tfrac{1}{2}\,b\xi \quad . \qquad 9.2.7$$

With these approximations, the quantities $c = \frac{1}{2}kd$ and $r_o = \frac{1}{2}d(1+\xi^2)^{\frac{1}{2}}$, the field is given by

$$\begin{aligned} \Xi_{mn}(x,y,\xi) = (c^{\frac{1}{2}}\, r_o^{-1})\ H_m(c^{\frac{1}{2}}\, x r_o^{-1})\ H_n(c^{\frac{1}{2}}\, y r_o^{-1}) \cdot \\ \cdot \exp\left[(-\,c/2)\ (r/r_o)^2\right] \cos\left[c\xi - (1 + m + n)\ \mathrm{Tan}^{-1}\,\xi\right] \end{aligned} \qquad 9.2.8$$

for the even mode, and cos → sin for the odd mode. The eigenvalue equation found by Boyd and Gordon (7) becomes, when written in terms of c and N ,

$$c = \frac{1}{4}\pi\,(2N + m + n + 1) \quad . \qquad 9.2.9$$

The two lowest order Hermite polynomials are given by (40)

$$H_o(x) = 1$$
$$H_1(x) = 2x \quad . \qquad 9.2.10$$

Thus the $\overline{E} = \overline{e}_y E_{1C}$ mode is given by

$$\overline{E} = \overline{e}_y(cx/r_o^2)\exp\left[(-c/2)(r/r_o)^2\right]\cos\left[\tfrac{1}{2}\pi\,(N+1)\,\xi - 2\,\mathrm{Tan}^{-1}\,\xi\right] \qquad 9.2.11$$

for the mode even about $\xi = 0$, and $\cos \rightarrow \sin$ for the odd mode. This mode is derivable from $m = 1$, $n = 1$ or 2 (for even and odd symmetry about $\xi = 0$) modes of Eq. 6.2.2 and 6.2.3 by the use of the e form of $m\varphi$ dependence, insertion of the asymptotic forms of the spheroidal functions of Eqs. 5.2.5 and 8.1,

$$S_{1n(\nu=0)} \sim (\pm 1)^{n-m}\,\alpha^{\frac{1}{2}}\,e^{-\frac{1}{2}\alpha}\,L_o^{\,1}(\alpha)$$

$$R^{(1)}_{1n(\nu=0)} \sim (cr_o)^{-1}\cos\left[c\xi - \tfrac{1}{2}\pi(n-1) - 2\,\mathrm{Tan}^{-1}\,\xi\right] \quad , \qquad 9.2.12$$

where $\alpha = c(r/r_o)^2$, use of (39)

$$L_o^{\,m}(x) = 1 \quad , \qquad 9.2.13$$

the eigenvalue equation, Eq. 8.4b for $\xi_o = 1$ written in terms of N

by the use of Eq. 8.7b

$$c_{N,m=1} = \tfrac{1}{2}\pi\,(N+1) \quad , \qquad 9.2.14$$

and

$$\bar{e}_y \approx -\,\bar{e}_\eta \sin\varphi + \bar{e}_\varphi \cos\varphi \quad . \qquad 9.2.15$$

Similarly, a superposition of Boyd and Gordon (7) modes

$$\bar{E} = -\,\bar{e}_x E_{01} + \bar{e}_y E_{10} \qquad 9.2.16$$

can be written

$$\bar{E} = \bar{e}_\varphi\, r^{-1}\,\alpha\, e^{-\frac{1}{2}\alpha} \cos\left[\tfrac{1}{2}\pi\,(N+1)\,\xi - 2\,\mathrm{Tan}^{-1}\,\xi\right] \qquad 9.2.17$$

for the mode even about $\xi = 0$, and $\cos \rightarrow \sin$ for the odd mode. This is the rotational TE mode for $n = 1$, for the even mode; $n = 2$ for the odd mode.

9.3 Correlation with Periodic Beam Phase Correction Analysis

The work of Goubau and Schwering (9) on periodically phase-corrected beams is, as has been recognized by others (8,52) applicable to laser cavity mode studies. Their analysis leads to hybrid waves which can be combined to form linearly polarized standing waves in the form

$$E_{mn}(x,y,z) = u^{-1}\,\delta^{\frac{1}{2}(m+1)}\,L_r^{\,m}(\delta)\,\exp\left(-\tfrac{1}{2}\delta\right)\cdot$$

$$\cdot\cos\left[kz + \tfrac{1}{2}\delta v - (2n + m + 1)\,\mathrm{Tan}^{-1}\,v\right]\cos m\varphi \qquad 9.3.1$$

and similarly with $\cos[\ ]\cos m\varphi \rightarrow \cos[\ ]\sin m\varphi$, $\sin[\ ]\cos m\varphi$, or $\sin[\ ]\sin m\varphi$, where

$$\delta = u^2/(1 + v^2)$$

$$u = \gamma_c(x^2 + y^2)^{\frac{1}{2}} \qquad 9.3.2$$

$$v = \gamma_o^{\,2}\,z/k$$

and γ_o is an arbitrary constant satisfying $\gamma_o^{\,2} \ll k^2$. By making the same substitution, $\xi = 2\,z/d$, γ_o is found to be $\gamma_o = k/c^{\frac{1}{2}}$, so that the inequality becomes $c \gg 1$, the same as that of the present analysis. The arbitrary constant γ_o is defined in terms of the oblate spheroidal parameter d . The approximation of Eqs. 9.2.6 and 9.2.7 inserted into Eq. 9.3.1 yield

$$E_{mn}(r,\xi) = r_o^{-1}\,(c\alpha)^{\frac{1}{2}m}\,L_n^{\,m}(\alpha)\,e^{-\frac{1}{2}c\alpha}\cdot$$

$$\cdot\cos\left[c\xi - (2n + m + 1)\,\mathrm{Tan}^{-1}\,\xi\right]\cos m\varphi \qquad 9.3.3$$

and permutation of the trigonometric functions. This expression is closely related to the expressions found in this paper.

9.4 Correlation with Parabolic Equation Method Analysis

Vainshtein (20) has used the parabolic equation method to analyze the spherical mirrors resonator. The electromagnetic field vectors are written as

$$\overline{E} = jk^{-1} \overline{\nabla} \times (\overline{\nabla} \times \overline{A})$$
$$\overline{H} = \overline{\nabla} \times \overline{A} \quad . \qquad 9.4.1$$

If $\overline{A}$ is an exact solution of the vector wave equation, then $\overline{E}$ can be written

$$\overline{E} = jk^{-1} (\overline{\nabla}(\overline{\nabla} \cdot \overline{A}) + k^2 \overline{A}) \quad . \qquad 9.4.2$$

If $\overline{H}$ is taken to have only an η or ξ component, and this component is taken to be Φ, a solution of the scalar wave equation, then the η and ξ components of $\overline{E}$ given by Eq. 9.4.1 and 9.4.2 differ by terms of order c^{-1}. The scalar wave equation is reduced, by neglecting terms of order c^{-1}, to a parabolic equation, which can be transformed into the Schrodinger temporal equation for an isotropic two-dimensional harmonic oscillator. Conversely, setting the two η or ξ components of $\overline{E}$ from Eq. 9.4.1 and 9.4.2 equal yields an equation for the η or ξ component of $\overline{A}$. By assuming that the coordinate system is roughly Cartesian, equations differing from the scalar wave equation are obtained. By reduction through dropping terms of order c^{-1}, it reduces to the previously found equation for the scalar wave function. This method seems less straightforward and less general than the approach taken in the present work.

PART II

DOMINANT MODE CALCULATIONS IN OUTPUT-COUPLED INFINITE STRIP MIRROR RESONATORS

CHAPTER TEN

INTRODUCTION

10.1 Review of the Field Numerical Calculations

The first numerical calculations on laser modes were carried out by Fox and Li (4) in their study of the possibility of a self-reproducing mode structure within a Fabry-Perot interferometer, when used as a low loss multimode optical cavity. The method of analysis was to consider the waves bouncing back and forth between the perfectly conducting mirrors as equivalent to a beam passing through apertures the shape of the mirrors in a periodic sequence of perfectly absorbing screens. By exciting the apertures system with an arbitrary beam and by letting the beam transit enough of the beam guide so that the higher loss modes die out, the lowest loss mode or modes would be left.

The analysis involves the scalarization of the Huyghens-Fresnel integral relating the field outside a closed surface to the values of the field and its normal derivative on the surface, which can be approximately done in the case of approximately transverse electromagnetic waves, when the wavelength of light is much less than the cavity dimensions. With this integral the traveling-wave field arriving at one mirror is related to the field leaving the other.

Since the field coordinates are infinite-dimensional variables, the complex field amplitudes are continuous functions. Solutions of the integral equations using continuous functions are or were not

known, so numerical techniques were necessary. The continuous functions were approximated by finite-dimensional vectors and the kernel of the integral equation by a matrix. Thus the integral equation relating continuous functions is converted to a matrix vector product equation. Successive multiplications of the initial vector by the matrix then would generate vectors in the space of the largest amplitude eigenvalue or eigenvalues.

Their results showed that there are in fact self-reproducing modes in this type of cavity, characterized by a definite mode structure, diffraction loss per transit, and phase shift per transit (the phase shift is such that it represents an increase in the phase velocity over that of a wave in free space, just as in the more familiar cylindrical waveguides).

With this method Fox and Li (4) studied the mode structure of the dominant modes in infinite strip, rectangular, and circular plane-parallel mirrors resonators, and confocal spherical mirrors resonators.

Goubau and Schwering (9), in their study of periodically phase-corrected beams in a system of thin lenses in apertures in perfectly absorbing screens, treated the equivalent of the non-confocal spherical mirrors resonator problem using the expansion-truncation method, in which the field function and the kernel are expanded in a convergent series of suitable orthogonal functions and the series is truncated at a suitable point. The resulting equation is again a matrix equation, becoming a matrix eigenvalue equation when the field functions are required to be equal within a complex constant, with the amplitudes of

the function expansion in the series as the components of the vector. Goubau and Schwering found only the eigenvalue of largest magnitude (lowest loss); Beier and Scheibe (57) solved for higher order eigenvalues using the same method.

Soohoo (12) considered the highly non-confocal spherical mirrors resonator, with the mirror separation much greater than the mirror radius. The matrix eigenvalue equation obtained was solved by iteration, using Franklin (58).

Fox and Li (10,11) used the iteration method to solve the case of resonators with mirrors of unequal radii of curvature and areas, and the iteration method described by Bodewig (59) for determining the eigenvalues of largest amplitude when their amplitudes are equal (this method is also used in Franklin (58)).

She and Heffner (14) propose the use of the expansion-truncation method and diagonalization of the characteristic matrix with plane-parallel circular mirrors, but perform no calculations with it. Bergstein and Schachter (15) carry out calculations with this method on plane-parallel infinite strip, rectangular, and circular mirrors resonators.

Gordon and Kogelnik (60) have shown that, for non-symmetric spherical mirror resonators, three rather than the expected five parameters of the system are sufficient to determine the mode patterns, diffraction losses, and resonant frequencies, thereby simplifying the calculations needed to predict the characteristics of the resonator.

Output Coupling

Boyd and Kogelnik (8) considered analytically the case of a rectangular shape, equal radii of curvature, confocal spherical mirrors resonator with a non-reflecting strip located centrally across one dimension of one mirror, and derived approximate expressions for the eigenvalues and eigenfunctions of the resonator.

Evtuhov and Neeland (61,62) have investigated the transverse and longitudinal mode structure in ruby lasers. One of their methods of transverse mode selection is to isolate the desired mode and prevent other modes from oscillating by shaving the mirror from one end of the ruby except in the area normally occupied by the desired mode. They found no significant increase in the threshold, effective control of the oscillation mode, and an increase in beam brightness; and the output beam remained diffraction-limited at pumping levels up to at least 2.5 times threshold. They did observe unexpected effects in the far field output pattern (63). Suematsu and Iga (64) and Siegman (65) found substantially the same results on the laser mode structure from shaving the mirror.

Patel et al (66) made the first use of output coupling by placing a small hole in the gold reflecting surface of a quartz mirror, in order to increase the laser output by increasing the reflectivity of the mirror without at the same time losing the transmitted power in absorption in the thick metal layer required for the high reflectivity. Qualitatively understandable effects on the mode structure due to the missing coating were evident.

La Tourette, Jacobs and Rabinowitz (67) used a small aluminum mirror as a means of output-coupling the laser power around its edges.

McCumber (15) has made calculations on the effect of output-coupling apertures on the confocal spherical mirrors resonator, using the kernel expansion-truncation method. The effect on the mode structure, the loss and phase shift, and the far field pattern was investigated.

10.2 Content of this Paper

The purpose of this work is to calculate, using an electronic computer, the characteristics of the dominant modes within infinite strip, plane-parallel mirrors, with output coupling.

The resonator to be studied has mirrors of equal width, each having a non-reflecting strip centered on each mirror. This is equivalent to a pair of infinite strip resonators, close enough to interact through diffraction coupling. As was previously pointed out, the black central strip represents a power loss to the resonator, while it is the output coupling mechanism from the standpoint of getting useful power into the beam.

CHAPTER ELEVEN

MASKED INFINITE STRIP MIRRORS

11.1 Physical Equation

In Appendix E is derived the equation relating the field function $u_2(x_2)$ at the "field" mirror of width b to the field function $u_1(x_1)$ on an identical "source" mirror a distance d away in the form

$$u_2(x_2) = (\lambda d)^{-\frac{1}{2}} \exp[j(\pi/4 - kd)] \int_{-b}^{b} dx_1 \; u_1(x_1) \exp[-jk(x_2 - x_1)^2/2d] \qquad 11.1.1$$

which is valid when the following conditions on the cavity dimensions are satisfied:

$$\lambda/d \ll 2\pi$$

$$4b^2/d^2 \ll 1 \qquad 11.1.2$$

$$b^2/\lambda d \ll d^2/8b^2 \quad .$$

The conversion to the case of a "source" mirror with a central black strip is accomplished by cutting that section out of the region of integration in Eq. 11.1.1. For a strip of half-width a, the integral equation becomes

$$u_2(x_2) = (\lambda d)^{-\frac{1}{2}} \exp[j(\pi/4 - kd)] \cdot$$

$$\cdot \int_{-b}^{-a} + \int_{+a}^{+b} dx_1 \exp[-jk(x_2 - x_1)^2/2d]\, u_1(x_1) \qquad 11.1.3$$

For an arbitrary field function $u_1(x_1)$ on the first mirror, the field on the mirror after the $(n - 1)$th transit is given by repeated application of the equation

$$u_n(x_n) = (\lambda d)^{-\frac{1}{2}} \exp[j(\pi/4 - kd)] \cdot$$

$$\cdot \int_{-b}^{-a} + \int_{a}^{b} dx_{n-1} \exp[-jk(x_n - x_{n-1})^2/2d]\, u_{n-1}(x_{n-1}) \qquad 11.1.4$$

This equation applies equally to the double infinite slit apertures in plane absorbing screens, with u_n being the field function in the nth aperture of the beam resulting from a field function u_1 in the first aperture.

If the concept of the dominant mode is realizable, then after some suitable number n of transits the field will reproduce itself within a constant factor at each transit. This can be written

$$u_n(x_n) = \gamma\, u_{n-1}(x_n) \quad , \qquad 11.1.5$$

which permits conversion of Eq. 11.1.4 into the integral eigenfunction-eigenvalue equation for the complex field amplitude with a complex eigenvalue from the symmetric, complex kernel derived from the masked

infinite strip plane-parallel mirrors resonator:

$$\gamma\, u_n(x_n) = (\lambda d)^{-\frac{1}{2}} \exp[j(\pi/4 - kd)] \cdot \cdot \left\{ \int_{-b}^{-a} + \int_{a}^{b} \right\} dx_{n-1} \exp[-jk(x_n - x_{n-1})^2/2d]\, u_n(x_{n-1}) \,. \qquad 11.1.6$$

Following the usual practice, the product kd will be assumed to be an integer times 2π, so that the calculated phase shifts will be relative to the geometrical phase shift of a plane wave in the distance d.

The resonator is invariant to reflection in the plane defined by the center lines of the black strips. The field functions will then have even or odd symmetry about this plane. With this symmetry condition,

$$u_n^{\pm}(x_n) = \pm u_n^{\pm}(-x_n) \quad , \qquad 11.1.7$$

where the plus sign signifies an even symmetry mode and the minus sign signifies an odd symmetry mode, Eq. 11.1.6 becomes

$$\gamma\, u_n^{\pm}(x_n) = (\lambda d)^{-\frac{1}{2}} \exp(j\pi/4) \int_a^b dx_{n-1} \cdot \cdot \left\{ \exp[-jk(x_n - x_{n-1})^2/2d] \pm \exp[-jk(x_n + x_{n-1})^2/2d] \right\} u_n^{\pm}(x_{n-1}) \qquad 11.1.8$$

and x_n takes on positive values only.

11.2 Dimensionless Equation

All the physics of the resonator, within the approximations given above, is in Eq. 11.1.8. To handle it mathematically, it is turned into a dimensionless equation, from which the significant parameters can be recognized. By defining the quantities

$$\begin{aligned} \alpha &= a/b \\ \beta &= b/(\lambda d)^{\frac{1}{2}} \\ \eta_n &= x_n/b \\ U_n(\eta_n) &= u_n(x_n) \quad , \end{aligned} \tag{11.2.1}$$

Equation 11.1.8 becomes

$$\begin{aligned} U_n^{\pm}(\eta_n) = \beta \exp(j\pi/4) \int_{\alpha}^{1} d\eta_{n-1} \cdot \\ \cdot \Big\{ \exp[-j\pi\beta^2(\eta_n - \eta_{n-1})^2] \\ \pm \exp[-j\pi\beta^2(\eta_n + \eta_{n-1})^2] \Big\} \; U_n^{\pm}(\eta_{n-1}) \quad . \end{aligned} \tag{11.2.2}$$

The quantities in Eq. 11.2.1 can take on values in the ranges

$$\begin{aligned} 0 \le \alpha < 1 \\ 0 \le \beta < \infty \\ \alpha \le \eta_n \le 1 \quad . \end{aligned} \tag{11.2.3}$$

The quantity β is related to the Fresnel number H for the unmasked infinite strip mirror by the relation

$$H = 2\beta^2 \quad . \qquad 11.2.4$$

11.3 Computer Equation

Equation 11.2.2 does not have exact solutions. In order to gain understanding of the physical problem it represents, it must be solved numerically. An electronic computer is ideally suited for handling matrix and vector operations; and, by converting the integral to a sum, Eq. 11.2.2 can be cast into this form.

The trapezoidal rule was chosen for conversion of the integral to a sum. Some check points were also calculated using Simpson's rule as a comparison, with no significant difference in the results. The trapezoidal rule is given by

$$\int_a^b f(x)dx \cong [(b - a)/(N - 1)] \sum_{i=1}^{N} c_i f(x_i) \quad , \qquad 11.3.1$$

where c_i is given by

$$\begin{aligned} c_i &= \tfrac{1}{2} \text{ if } i = 1 \text{ or } N \\ &= 1 \text{ for all other } i \end{aligned} \qquad 11.3.2$$

and x_i is given by

$$x_i = a + (i - 1)(b - a)/(N - 1) \quad . \qquad 11.3.3$$

Then by writing

$$\eta_n \rightarrow \eta(J) = \alpha + (J - 1)(1 - \alpha)/(N - 1)$$

$$\eta_{n-1} \rightarrow \eta(I) = \alpha + (I - 1)(1 - \alpha)/(N - 1)$$

$$U_n(\eta_n) \rightarrow U(J) \ , \ U_n(\eta_{n-1}) \rightarrow U(I)$$

$$K^{\pm}(J,I) = c(I) \left\{ \exp[-j\pi\beta^2(\eta(J) - \eta(I))^2] \right. \qquad 11.3.4$$

$$\left. \pm \exp[-j\pi\beta^2(\eta(J) + \eta(I))^2] \right\}$$

$$c(I) = \tfrac{1}{2} \text{ if } I = 1 \text{ or } N$$

$$= 1 \text{ for all other } I$$

$$\lambda = \gamma \exp(-j\pi/4)(N - 1)/\beta(1 - \alpha) \ ,$$

Eq. 11.2.2 becomes a matrix eigenvalue equation:

$$\lambda \, U^{\pm}(J) = \sum_{I=1}^{N} K^{\pm}(J,I) \, U^{\pm}(I) \ . \qquad 11.3.5$$

The kernel $K^{\pm}(J,I)$ is a complex symmetric matrix of dimensions $N \times N$, and the vector $U^{\pm}(I)$ is a complex vector of dimension N. The eigenvalue λ and the vector $U^{\pm}(J)$ are the desired results of the eigenvalue problem for the known kernel $K^{\pm}(J,I)$.

CHAPTER TWELVE

MASKED INFINITE STRIP MIRRORS CALCULATIONS

12.1 Parameters

Calculations were performed by the methods and programs described in Appendix F. The parameters used were $\beta = 0.5$, 1.0, and 2.0, and $\alpha = 0.0$, 0.1, 0.2, 0.4, and 0.8.

The program did not solve the eigenvalue problem for the set of parameters $\beta = 2.0$ and $\alpha = 0.0$. This point was taken from a set of points run with a different program, written to verify the results of Fox and Li (4).

12.2 Results

Some of the results of the computer calculations are given in Table 1 and Fig. 5-15.

Table 1 contains the percent relative power loss per transit and the phase shift per transit relative to the phase shift of a plane wave. Figure 5 is a plot of the power loss data, and Fig. 6 is a plot of the phase shift data.

Figures 7-10 show the relative amplitudes and phases of the even and odd symmetry field functions for $\beta = 2.0$ and various α.

Figures 11-14 show the relative amplitudes and phases of the even and odd symmetry field functions for $\alpha = 0.1$ and various β.

β	α	Symmetry	PLOSS	PHASH
0.5	0.0	E	32.24	21.07
		O	82.64	84.00
	0.1	E	48.09	18.27
		O	82.67	83.94
	0.2	E	61.95	14.80
		O	82.91	83.53
	0.4	E	83.24	5.61
		O	84.86	80.51
	0.8	E	99.62	-23.90
		O	96.48	61.34
1.0	0.0	E	8.17	7.83
		O	27.10	30.93
	0.1	E	40.83	8.33
		O	27.79	30.82
	0.2	E	75.39	21.91
		O	32.88	30.06
	0.4	E	63.67	40.54
		O	65.04	25.48
	0.8	E	96.79	82.02
		O	91.32	31.01
2.0	0.0	E	1.30	2.36
		O	4.80	9.45
	0.1	E	16.92	9.88
		O	5.17	9.43
	0.2	E	11.68	11.82
		O	13.18	10.29
	0.4	E	22.86	16.74
		O	25.01	16.14
	0.8	E	85.60	40.85
		O	82.72	39.74

Table 1. PLOSS is the percent relative power loss per transit; PHASH is the degrees of phase shift relative to a plane wave; of the dominant mode in a masked infinite strip plane-parallel mirrors resonator.

Fig. 5. Percent power loss per transit of the dominant mode in the masked infinite strip plane-parallel mirrors resonator, for various β^2 , α , and symmetry.

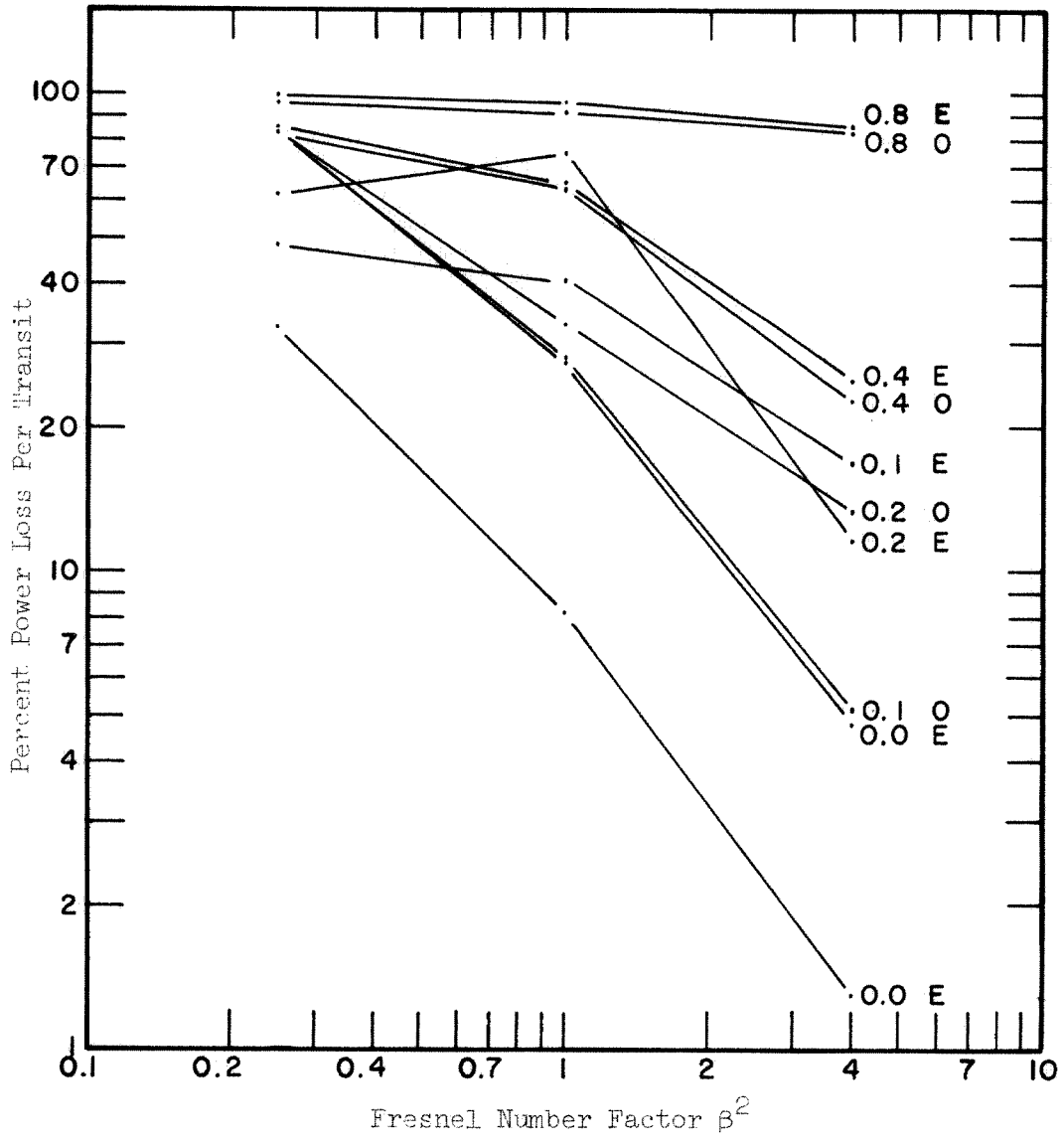

Fig. 6. Degrees of phase shift relative to a plane wave of the dominant mode in the masked infinite strip plane-parallel mirrors resonator, for various β^2 , α , and symmetry. The 0.0 0 points coincide with the 0.1 0 points.

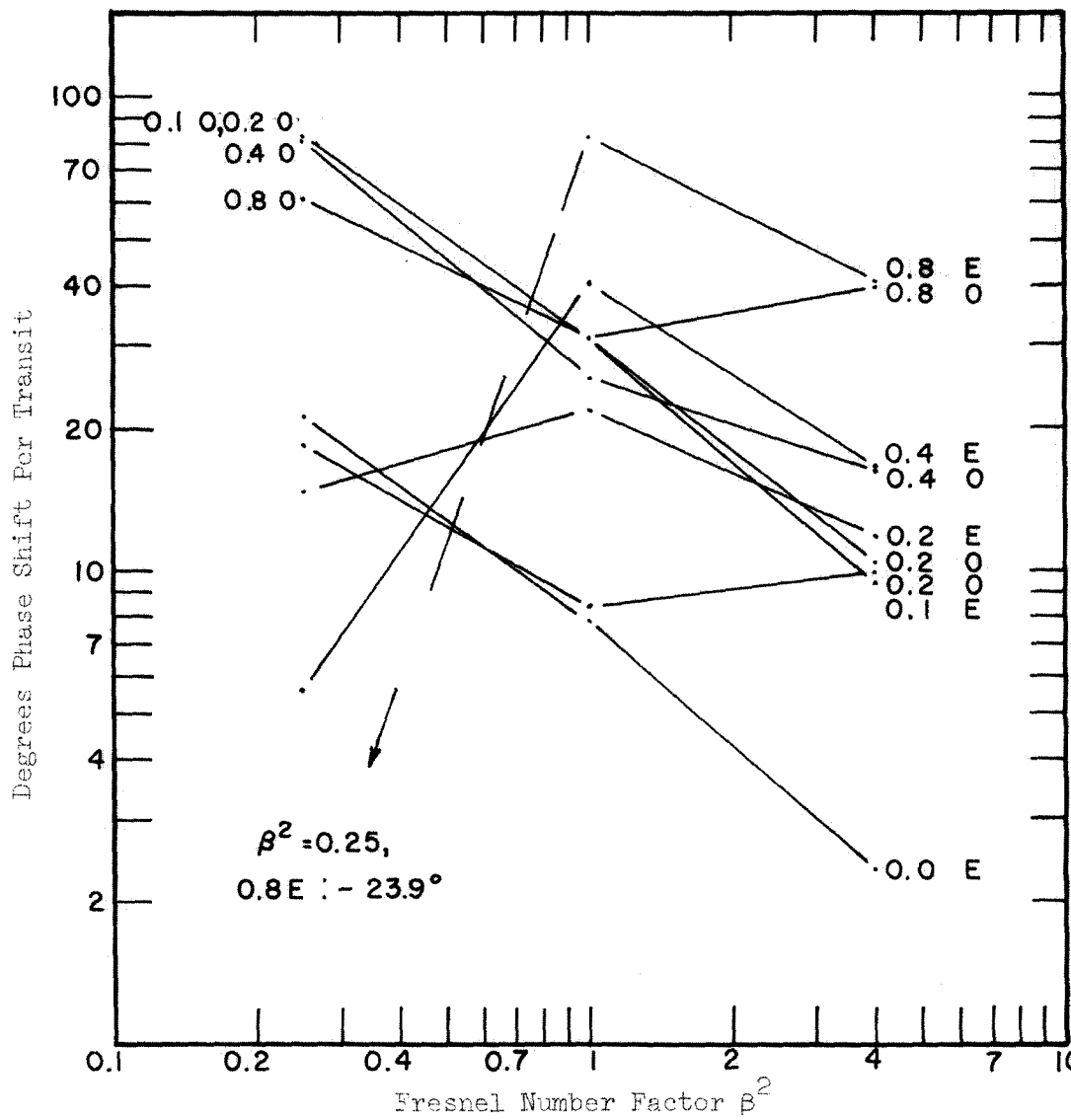

Fig. 7. Relative amplitude of the field function on the mirrors of the dominant mode in the masked infinite strip plane-parallel mirrors resonator, for $\beta = 2.0$, even symmetry, and various α.

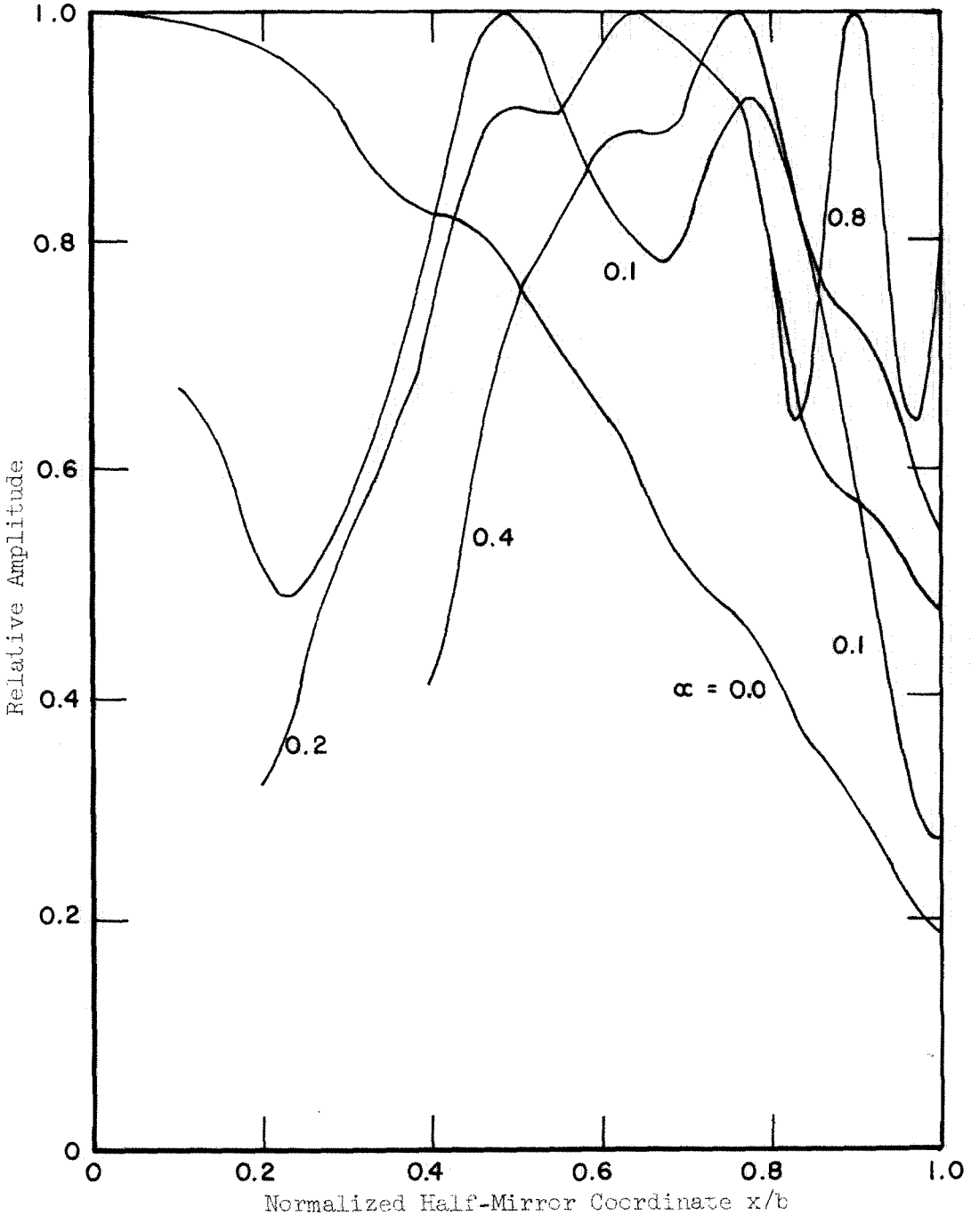

Fig. 8. Relative phase of the field function on the mirrors of the dominant mode in the masked infinite strip plane-parallel mirrors resonator, for $\beta = 2.0$, even symmetry and various α.

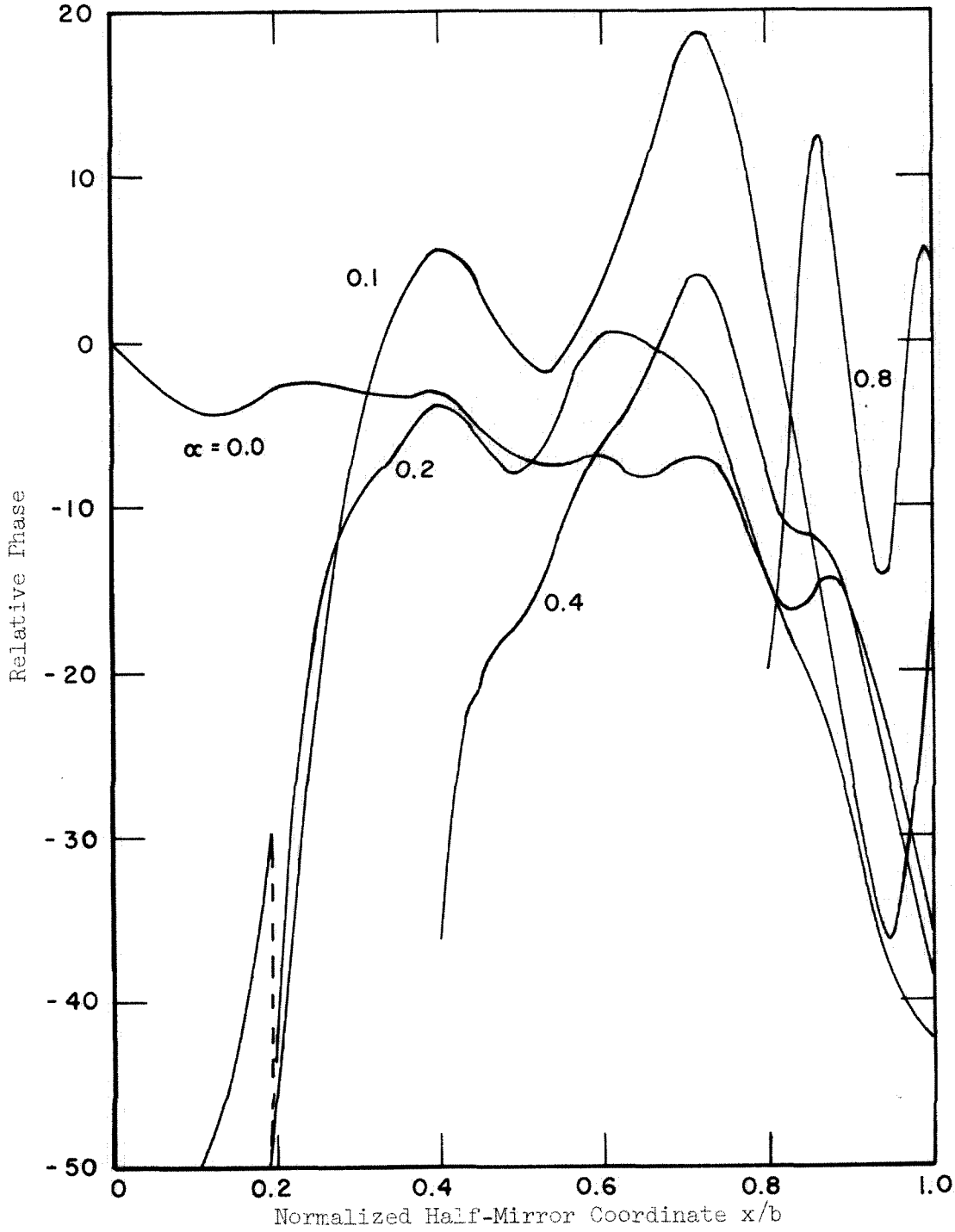

Fig. 9. Relative amplitude of the field function on the mirrors of the dominant mode in the masked infinite strip plane-parallel mirrors resonator, for $\beta = 2.0$, odd symmetry, and various α.

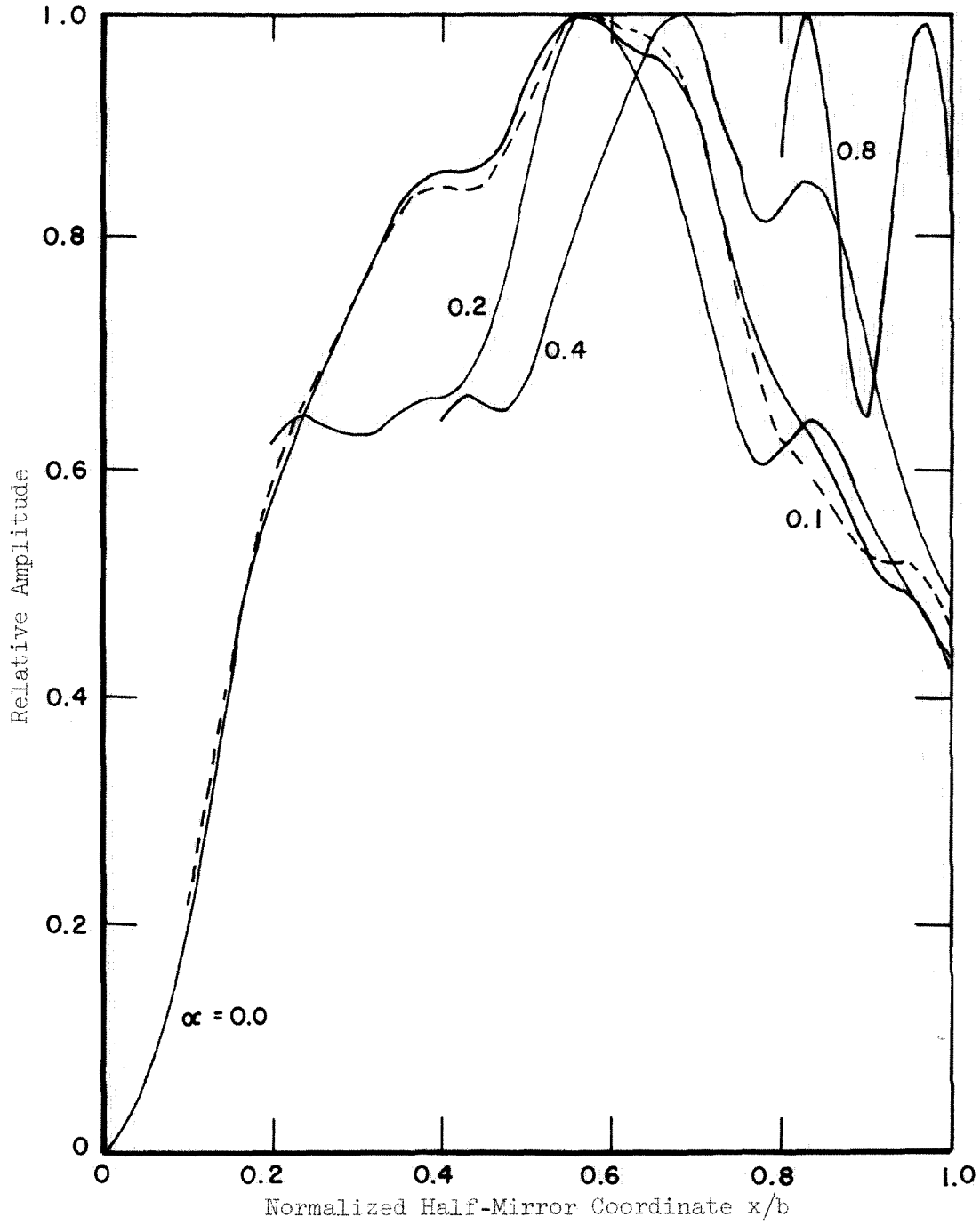

Fig. 10. Relative phase of the field function on the mirrors of the dominant mode in the masked infinite strip resonator, for $\beta = 2.0$, odd symmetry, and various α.

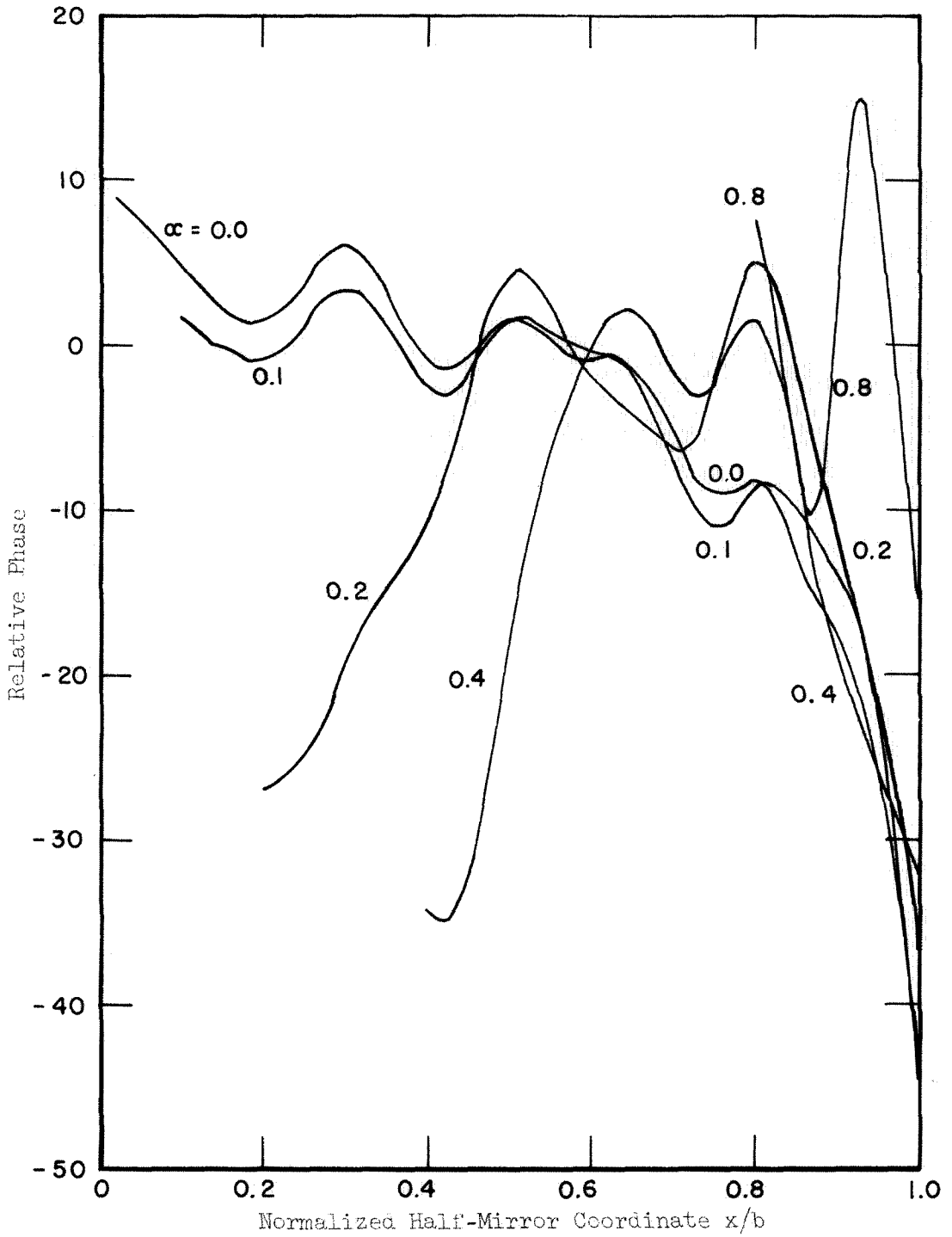

Fig. 11. Relative amplitude of the field function on the mirrors of the dominant mode in the masked infinite strip resonator, for $\alpha = 0.1$, even symmetry, and various β.

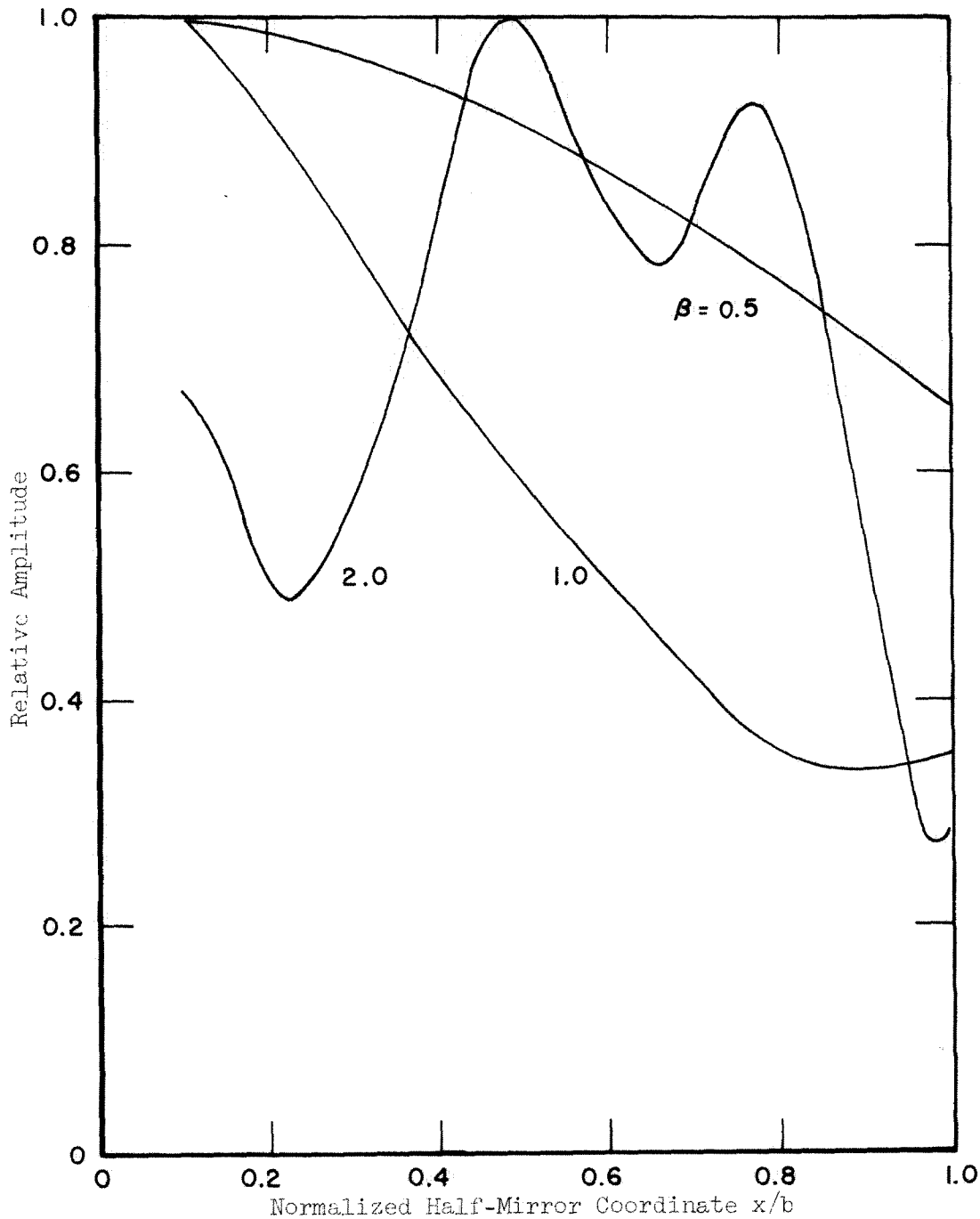

Fig. 12. Relative phase of the field function on the mirrors of the dominant mode in the masked infinite strip resonator, for $\alpha = 0.1$, even symmetry, and various β.

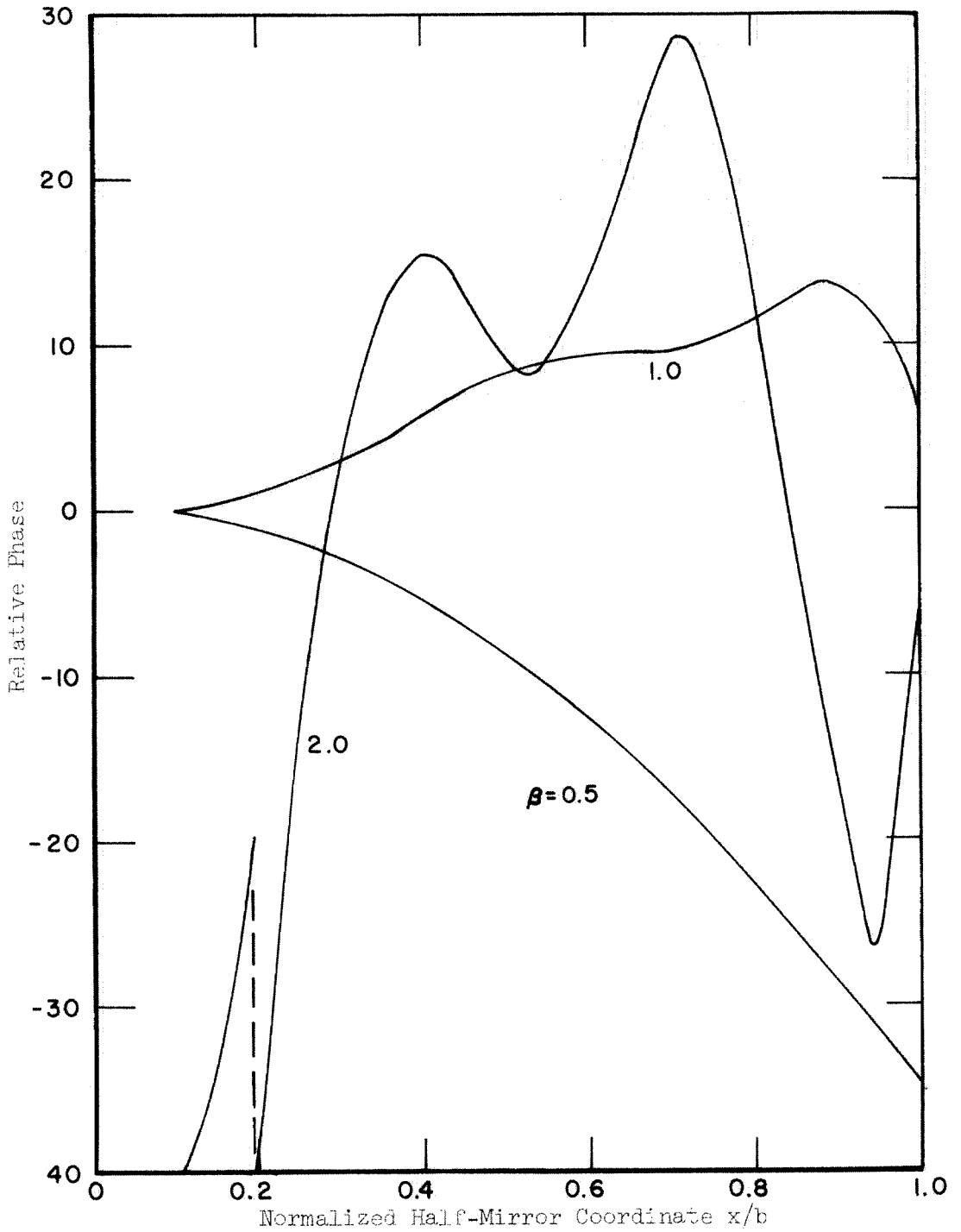

Fig. 13. Relative amplitude of the field function on the mirrors of the dominant mode in the masked infinite strip resonator, for $\alpha = 0.1$, odd symmetry, and various β.

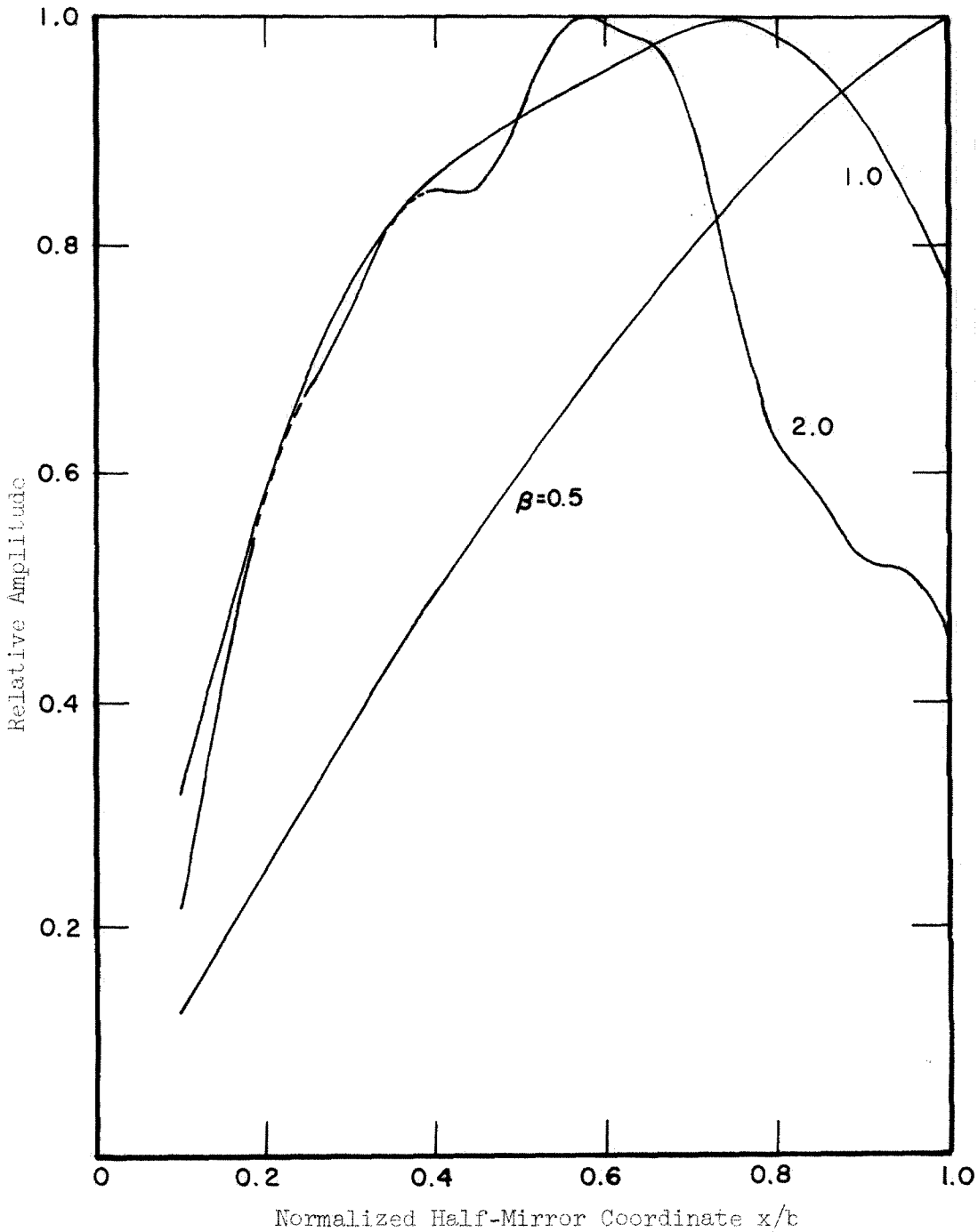

Fig. 14. Relative phase of the field function on the mirrors of the dominant mode in the masked infinite strip resonator, for $\alpha = 0.1$, odd symmetry, and various β.

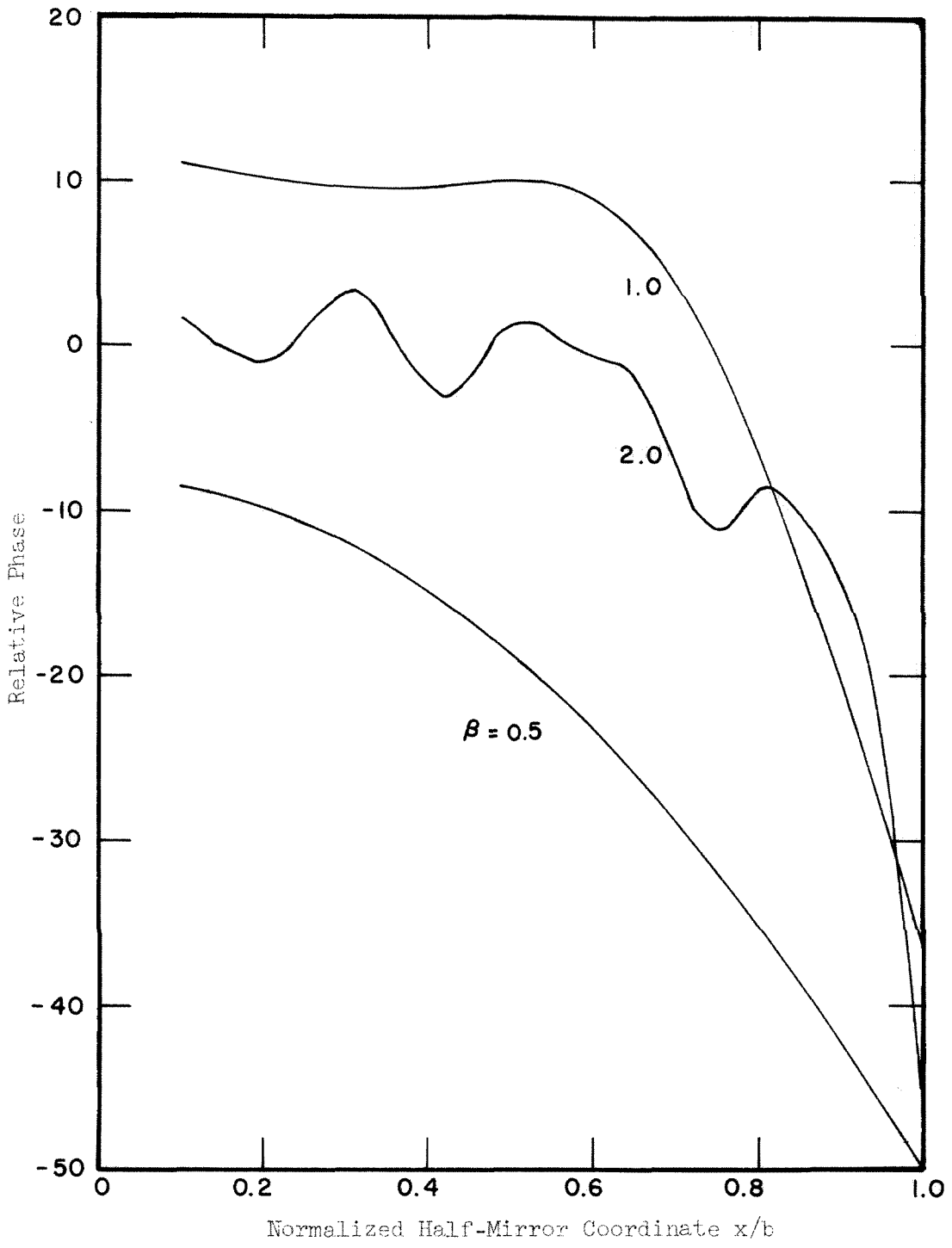

12.3 Discussion of Results

The results of the case $\alpha = 0.0$ agree excellently with the results of Fox and Li (4) for the non-masked mirrors resonator.

It can be seen that the odd symmetry modes are not as strongly affected by the masking strip as are the even symmetry modes. The additional power loss and phase shift change rapidly with α for even symmetry and slowly with α for odd symmetry, particularly for small and large β. The field function for even symmetry is similarly much more affected by non-zero α than is the odd symmetry field function.

This can be qualitatively understood from the standpoint of perturbations. The odd symmetry modes have a smaller proportion of their field strength within the masked strip, particularly for small β, so that the masking has less effect on the odd symmetry modes. For small β, the even symmetry modes have broad maxima at the center of the masked strip, so that the power loss from an even symmetry mode should be approximately proportional to α for small α. The odd symmetry modes for small β are linear through zero at the center of the masked strip, so that the power loss should be approximately proportional to α^2 for small α.

The data in Table 1 shows that the conclusions given above are roughly correct. It is of interest to consider how well the power loss can be estimated by using perturbation. For the $\beta = 0.5$, $\alpha = 0.0$ even symmetry resonator mode the power loss per transit is 32%, so that 68% of the power on one mirror is incident on the other. The field function for this resonator is not shown in the figures of

this paper, but is closely approximated by the function for the $\beta = 0.5$, $\alpha = 0.1$ resonator. By squaring the amplitude curve and estimating its area, it is seen that about one-eighth of the power on the mirror lies in the $\alpha = 0.1$ zone. Thus the perturbation estimate of the additional power loss is one-eighth of 68%, or approximately 9%. It can be seen from Table 1 that the actual additional power loss due to masking for this case is 16%. The perturbation estimate is an order of magnitude, but not an accurate estimate, for the values of α used in this paper.

At large values of α, the two halves of the resonator become less coupled, beginning to appear as two isolated resonators with narrow mirrors, with diffraction coupling between the resonators. The resonators are still within the configuration of the unmasked resonator, for which it was assumed that all parts of the mirrors were diffraction coupled, so that the less coupling does not extend to zero coupling. This can be seen by examination of the field functions for even and odd symmetry for $\alpha = 0.8$. Though the power losses are about the same, the phase shift per transit and the field functions differ markedly.

The power losses for large values of α are greater for the even symmetry modes than for the odd symmetry modes. This can be understood in terms of the field on the masked strip containing more power in the even symmetry mode than in the odd symmetry mode. The field on the center of the masked strip is usually not zero in the even symmetry mode, and is always zero in the odd symmetry mode.

APPENDICES

PART I

APPENDIX A

VECTOR WAVE EQUATION

Maxwell's equations relating the electric field intensity vector $\overline{E}(\overline{r},t)$, the electric displacement vector $\overline{D}(\overline{r},t)$, the magnetic induction vector $\overline{B}(\overline{r},t)$, and the magnetic field intensity vector $\overline{H}(\overline{r},t)$ are

$$\overline{\nabla} \times \overline{E}(\overline{r},t) = -\frac{\partial \overline{B}}{\partial t}(\overline{r},t)$$

$$\overline{\nabla} \times \overline{H}(\overline{r},t) = \overline{J}(\overline{r},t) + \frac{\partial \overline{D}}{\partial t}(\overline{r},t) \qquad \text{A.1}$$

$$\overline{\nabla} \cdot \overline{D}(\overline{r},t) = \rho(\overline{r},t)$$

$$\overline{\nabla} \cdot \overline{B}(\overline{r},t) = 0$$

where $\rho(\overline{r},t)$ is the electric charge density and $\overline{J}(\overline{r},t)$ is the conduction and convection current density. $\overline{D}(\overline{r},t)$ and $\overline{E}(\overline{r},t)$, and $\overline{B}(\overline{r},t)$ and $\overline{H}(\overline{r},t)$, are related by the constitutive relations

$$\overline{D}(\overline{r},t) = \epsilon\, \overline{E}(\overline{r},t)$$

$$\overline{B}(\overline{r},t) = \mu\, \overline{H}(\overline{r},t) \qquad \text{A.2}$$

where, for the case of interest here, namely, a homogeneous, isotropic, linear medium, ϵ and μ are scalar constants independent of position. In a conductive medium, $\overline{J}(\overline{r},t)$ is related to $\overline{E}(\overline{r},t)$ by Ohm's law,

$$\bar{J}(\bar{r},t) = \sigma\, \bar{E}(\bar{r},t) \quad . \tag{A.3}$$

The conductivity σ is assumed to be zero, and no convection current or electric charge is introduced.

As a consequence of the above restrictions, Maxwell's equations become

$$\begin{aligned}
\bar{\nabla} \times \bar{E}(\bar{r},t) &= -\mu \frac{\partial \bar{H}}{\partial t}(\bar{r},t) \\
\bar{\nabla} \times \bar{H}(\bar{r},t) &= +\epsilon \frac{\partial \bar{E}}{\partial t}(\bar{r},t) \\
\bar{\nabla} \cdot \bar{E}(\bar{r},t) &= 0 \\
\bar{\nabla} \cdot \bar{H}(\bar{r},t) &= 0 \quad .
\end{aligned} \tag{A.4}$$

The solutions are written in the separated form

$$\begin{aligned}
\bar{E}(\bar{r},t) &= \bar{E}(\bar{r})\, e^{j\omega t} \\
\bar{H}(\bar{r},t) &= \bar{H}(\bar{r})\, e^{j\omega t} \quad .
\end{aligned} \tag{A.5}$$

Equations A.4 then become

$$\begin{aligned}
\bar{\nabla} \times \bar{E}(\bar{r}) &= -j\omega\mu\, \bar{H}(\bar{r}) \\
\bar{\nabla} \times \bar{H}(\bar{r}) &= +j\omega\epsilon\, \bar{E}(\bar{r}) \\
\bar{\nabla} \cdot \bar{E}(\bar{r}) &= 0 \\
\bar{\nabla} \cdot \bar{H}(\bar{r}) &= 0 \quad .
\end{aligned} \tag{A.6}$$

By taking the curl of both sides, the first two equations become

$$\bar{\nabla} \times (\bar{\nabla} \times \bar{E}(\bar{r})) = - j\omega\mu \, \bar{\nabla} \times \bar{H}(\bar{r})$$

$$\bar{\nabla} \times (\bar{\nabla} \times \bar{H}(\bar{r})) = + j\omega\epsilon \, \bar{\nabla} \times \bar{E}(\bar{r}) \; . \qquad \text{A.7}$$

The left-hand sides can be transformed with the use of the vector identity

$$\bar{\nabla} \times (\bar{\nabla} \times \bar{u}) = \bar{\nabla}(\bar{\nabla} \cdot \bar{u}) - \nabla^2 \bar{u} \quad ; \qquad \text{A.8}$$

and, with the insertion of Eq. A.4, the result is

$$\nabla^2 \bar{E}(\bar{r}) + k^2 \bar{E}(\bar{r}) = 0$$

$$\nabla^2 \bar{H}(\bar{r}) + k^2 \bar{H}(\bar{r}) = 0 \quad , \qquad \text{A.9}$$

or, equivalently,

$$\bar{\nabla} \times (\bar{\nabla} \times \bar{E}(\bar{r})) - k^2 \bar{E}(\bar{r}) = 0$$

$$\bar{\nabla} \times (\bar{\nabla} \times \bar{H}(\bar{r})) - k^2 \bar{H}(\bar{r}) = 0 \quad , \qquad \text{A.10}$$

with the side conditions

$$\bar{\nabla} \cdot \bar{E}(\bar{r}) = 0$$

$$\bar{\nabla} \cdot \bar{H}(\bar{r}) = 0 \quad , \qquad \text{A.11}$$

where

$$k^2 = \omega^2 \mu\epsilon \quad . \qquad \text{A.12}$$

APPENDIX B

VECTOR WAVE FUNCTION SOLUTION

In Appendix A it was shown that for the physical problem of interest the equations governing the electromagnetic fields are (exp (jωt) time dependence assumed)

$$\begin{aligned}
&\bar{\nabla} \times (\bar{\nabla} \times \bar{E}(\bar{r})) - \omega^2 \mu\epsilon \, \bar{E}(\bar{r}) = 0 \\
&\bar{\nabla} \times (\bar{\nabla} \times \bar{H}(\bar{r})) - \omega^2 \mu\epsilon \, \bar{H}(\bar{r}) = 0 \\
&\bar{\nabla} \cdot \bar{E}(\bar{r}) = 0 \\
&\bar{\nabla} \cdot \bar{H}(\bar{r}) = 0 \quad .
\end{aligned} \tag{B.1}$$

The electromagnetic field vectors can be given in general in the form

$$\begin{aligned}
&\bar{E}(\bar{r},t) = - \frac{\partial \bar{A}}{\partial t} (\bar{r},t) - \bar{\nabla} \psi \, (\bar{r},t) \\
&\bar{B}(\bar{r},t) = \bar{\nabla} \times \bar{A}(\bar{r},t)
\end{aligned} \tag{B.2}$$

or, with the exp (jωt) time dependence,

$$\begin{aligned}
&\bar{E}(\bar{r}) = - j\omega \bar{A}(\bar{r}) - \bar{\nabla} \psi \, (\bar{r}) \\
&\bar{B}(\bar{r}) = \bar{\nabla} \times \bar{A}(\bar{r}) \quad .
\end{aligned} \tag{B.3}$$

Smythe (53) shows that, when all charges are confined to perfect conductors, the electric potential can be set equal to zero; and the vector

potential can be required to be solenoidal. Then $\bar{E}(\bar{r})$ and $\bar{H}(\bar{r})$ are given by

$$\bar{E}(\bar{r}) = - j\omega\bar{A}(\bar{r})$$
$$\bar{H}(\bar{r}) = \mu^{-1} \bar{\nabla} \times \bar{A}(\bar{r}) \quad , \tag{B.4}$$

and the condition

$$\bar{\nabla} \cdot \bar{A}(\bar{r}) = 0 \tag{B.5}$$

guarantees solenoidal $\bar{E}(\bar{r})$ and $\bar{H}(\bar{r})$. The equation governing $\bar{A}(\bar{r})$ is, from Eq. B.1, with $k^2 = \omega^2\mu\epsilon$,

$$\bar{\nabla} \times (\bar{\nabla} \times \bar{A}(\bar{r})) - k^2 \bar{A}(\bar{r}) = 0 \quad . \tag{B.6}$$

Since $\bar{A}(\bar{r})$ can be required to be solenoidal, it can be written in the form

$$\bar{A}(\bar{r}) = \bar{\nabla} \times \bar{W} \quad . \tag{B.7}$$

Smythe (54) shows that the particular vector

$$\bar{W} = \bar{u}\, W_1 + \bar{u} \times \bar{\nabla}\, W_2 \quad , \tag{B.8}$$

where $\bar{u}$ is an arbitrary constant vector on the radius vector, is particularly convenient. The result of the operation curl $\bar{A}(\bar{r})$ is

$$\bar{\nabla} \times (\bar{\nabla} \times \bar{A}(\bar{r})) = - \bar{\nabla} \times [\bar{u}\, \nabla^2 W_1 + \bar{u} \times \bar{\nabla}(\nabla^2 W_2)] \quad , \tag{B.9}$$

so that Eq. B.6 becomes

$$\bar{\nabla} \times [\bar{u}(\nabla^2 W_1 + k^2 W_1) + \bar{u} \times \bar{\nabla}(\nabla^2 W_2 + k^2 W_2)] = 0 \ . \qquad \text{B.10}$$

Thus, if W_1 and W_2 are solutions of the scalar wave equations,

$$\begin{aligned} \nabla^2 W_1 + k^2 W_1 &= 0 \\ \nabla^2 W_2 + k^2 W_2 &= 0 \ , \end{aligned} \qquad \text{B.11}$$

solutions to the vector wave equation can be written as

$$\bar{A}(\bar{r}) = \bar{\nabla} \times [\bar{u} W_1 + \bar{u} \times \bar{\nabla} W_2] \ . \qquad \text{B.12}$$

This is two separate solutions, since W_1 or W_2 can separately be set equal to zero. Thus we have two forms for $\bar{A}(\bar{r})$,

$$\begin{aligned} \bar{A}_1(\bar{r}) &= \bar{\nabla} \times (\bar{u} W_1) = \bar{\nabla} W_1 \times \bar{u} \ , \\ \bar{A}_2(\bar{r}) &= \bar{\nabla} \times (\bar{u} \times \bar{\nabla} W_2) \ . \end{aligned} \qquad \text{B.13}$$

By considering the quantities $\bar{u} \cdot \bar{A}$ and $\bar{u} \cdot (\bar{\nabla} \times \bar{A})$, it can be seen that W_1 produces no $\bar{A}$ in the direction of $\bar{u}$, and that W_2 produces no $\bar{\nabla} \times \bar{A}$ in the direction of $\bar{u}$.

APPENDIX C

ROTATIONALLY SYMMETRIC SOLUTIONS OF THE VECTOR WAVE EQUATION

In Appendix A it was shown that the electric field intensity vector $\overline{E}(\overline{r})$ and the magnetic field intensity vector $\overline{H}(\overline{r})$ satisfies the pair of equations

$$\overline{\nabla} \times \overline{E}(\overline{r}) = - j\omega\mu \, \overline{H}(\overline{r})$$

$$\overline{\nabla} \times \overline{H}(\overline{r}) = + j\omega\epsilon \, \overline{E}(\overline{r}) \quad . \qquad \text{C.1}$$

The spheroidal coordinate systems do not permit separation of a general solution of the vector Helmholtz equation in a form suitable for matching boundary conditions (27,28). For the special case of fields with rotational symmetry about the axis, Eq. C.1 can be solved in a form suitable for matching boundary conditions on a spheroid (41-49). Equations C.1 are a set of six coupled equations:

$$\frac{\partial}{\partial \xi} (h_\varphi E_\varphi) - \frac{\partial}{\partial \varphi} (h_\xi E_\xi) + j\omega\mu \, h_\xi \, h_\varphi \, H_\eta = 0$$

$$\frac{\partial}{\partial \varphi} (h_\eta E_\eta) - \frac{\partial}{\partial \eta} (h_\varphi E_\varphi) + j\omega\mu \, h_\eta \, h_\varphi \, H_\xi = 0 \qquad \text{C.2a}$$

$$\frac{\partial}{\partial \eta} (h_\xi E_\xi) - \frac{\partial}{\partial \xi} (h_\eta E_\eta) + j\omega\mu \, h_\eta \, h_\xi \, H_\varphi = 0$$

$$\frac{\partial}{\partial \xi}(h_\varphi H_\varphi) - \frac{\partial}{\partial \varphi}(h_\xi H_\xi) - j\omega\epsilon\, h_\xi h_\varphi E_\eta = 0$$

$$\frac{\partial}{\partial \varphi}(h_\eta H_\eta) - \frac{\partial}{\partial \eta}(h_\varphi H_\varphi) - j\omega\epsilon\, h_\eta h_\varphi E_\xi = 0 \qquad \text{C.2b}$$

$$\frac{\partial}{\partial \eta}(h_\xi H_\xi) - \frac{\partial}{\partial \xi}(h_\eta H_\eta) - j\omega\epsilon\, h_\eta h_\xi E_\varphi = 0 \quad .$$

The scale factors h_i are independent of φ. If E_η, E_ξ, H_η, and H_ξ are required to be independent of φ, then the set of six coupled equations breaks into two uncoupled sets of three coupled equations each:

$$\left.\begin{aligned} \frac{\partial}{\partial \eta}(h_\varphi E_\varphi) + j\omega\mu\, h_\xi h_\varphi H_\eta &= 0 \\ -\frac{\partial}{\partial \eta}(h_\varphi E_\varphi) + j\omega\mu\, h_\eta h_\varphi H_\xi &= 0 \\ \frac{\partial}{\partial \eta}(h_\xi H_\xi) - \frac{\partial}{\partial \xi}(h_\eta H_\eta) - j\omega\epsilon\, h_\eta h_\xi E_\varphi &= 0 \end{aligned}\right\} \text{TE} \qquad \text{C.3a}$$

$$\left.\begin{aligned} \frac{\partial}{\partial \xi}(h_\varphi H_\varphi) - j\omega\epsilon\, h_\xi h_\varphi E_\eta &= 0 \\ -\frac{\partial}{\partial \eta}(h_\varphi E_\varphi) - j\omega\epsilon\, h_\eta h_\varphi E_\xi &= 0 \\ \frac{\partial}{\partial \eta}(h_\xi E_\xi) - \frac{\partial}{\partial \xi}(h_\eta E_\eta) + j\omega\mu\, h_\eta h_\xi H_\varphi &= 0 \quad . \end{aligned}\right\} \text{TM} \qquad \text{C.3b}$$

The transverse electric vector set has $\overline{E} \equiv \overline{e}_\varphi E_\varphi(\eta,\xi)$; the

transverse magnetic vector set has $\overline{H} \equiv \overline{e}_{\varphi} H_{\varphi}(\eta,\xi)$. Each set can be solved for the φ component. Writing $\Phi(\eta,\xi)$ for the φ component and inserting the scale factors in both sets yields the same equation for Φ :

$$\frac{\partial}{\partial\eta}\left[(1-\eta^2)\frac{\partial\Phi}{\partial\eta}\right]+\frac{\partial}{\partial\xi}\left[(\xi^2+1)\frac{\partial\Phi}{\partial\xi}\right]-\frac{\xi^2+\eta^2}{(\xi^2+1)(1-\eta^2)}\Phi+\frac{k^2d^2}{4}(\xi^2+\eta^2)\Phi=0. \qquad C.4$$

Comparing this with the scalar Helmholtz equation

$$\nabla^2 \Psi + k^2 \Psi = 0 \qquad C.5$$

which upon insertion of the scale factors becomes

$$\frac{\partial}{\partial\eta}\left[(1-\eta^2)\frac{\partial\Psi}{\partial\eta}\right]+\frac{\partial}{\partial\xi}\left[(\xi^2+1)\frac{\partial\Psi}{\partial\xi}\right]+\frac{\xi^2+\eta^2}{(\xi^2+1)(1-\eta^2)}\frac{\partial^2\Psi}{\partial\varphi^2}+\frac{k^2d^2}{4}(\xi^2+\eta^2)\Psi=0 \qquad C.6$$

shows that the solution for Φ is the solution for Ψ ,

$$\Psi(-jc,\eta,j\xi) = \sum_{m,n} a_{mn}\Psi_{mn}(-jc,\eta,j\xi) \quad ,$$

$$\Psi_{mn}(-jc,\eta,j\xi) = S_{mn}(-jc,\eta)R_{mn}(-jc,j\xi)\begin{Bmatrix}\sin\\ \cos\end{Bmatrix} m\varphi \quad , \qquad C.7$$

with no φ dependence and m set equal to one:

$$\Phi\ (-jc,\eta,j\xi) = \sum_n b_n\ \Phi_n\ (-jc,\eta,j\xi)\quad ,$$

$$\Phi_n(-jc,\eta,j\xi) = S_{ln}(-jc,\eta)\ R_{ln}(-jc,j\xi)\quad . \qquad \text{C.8}$$

The angular function $S_{mn}(-jc,\eta)$ and the radial function $R_{mn}(-jc,j\xi)$ are the solutions of the equations

$$\frac{d}{d\eta}\left[(1-\eta^2)\frac{d}{d\eta}S_{mn}(-jc,\eta)\right] + \left[\lambda_{mn} + c^2\eta^2 - \frac{m^2}{1-\eta^2}\right] S_{mn}(-jc,\eta) = 0 \qquad \text{C.9}$$

$$\frac{d}{d\xi}\left[(\xi^2+1)\frac{d}{d\xi}R_{mn}(-jc,j\xi)\right] - \left[\lambda_{mn} - c^2\xi^2 - \frac{m^2}{\xi^2+1}\right] R_{mn}(-jc,j\xi) = 0\quad . \qquad \text{C.10}$$

The quantity c is a dimensionless parameter given by

$$c = \frac{kd}{2}\quad . \qquad \text{C.11}$$

The numbers m and n are positive integers or zero, with $n \geq m$.

The η and ξ components of the electromagnetic fields are given by the use of Eq. C.3 with the φ components of Eq. C.8.

APPENDIX D

LIGHT SCATTERING FROM DIELECTRIC FILM LASER MIRRORS

The following pages are a reproduction of the Scientific Report No. 1 from the Quantum Electronics Laboratory of California Institute of Technology, titled "Light Scattering from Dielectric Film Laser Mirrors," dated September 1, 1962.

The results of this work are verified by the recent work of D. L. Perry (55). His work showed that the scattering spots are particles of the dielectric being deposited. By using the dielectric material in chunks instead of the usual powder form, preparing them properly, and evaporating them at a precise temperature below the melting point, the number of large particles is greatly reduced. The technique of observing the scattered light as a measure of the mirror quality is being used in his work.

An additional reference on dielectric films is Heavens (56).

CALIFORNIA INSTITUTE OF TECHNOLOGY

Quantum Electronics Laboratory

LIGHT SCATTERING FROM DIELECTRIC FILM LASER MIRRORS*

Walter A. Specht, Jr.

Contract No. AF19(604)-8052
Project 4600
Task 460006

Scientific Report No. 1

1 September 1962

Prepared for

Electronics Research Directorate
Air Force Cambridge Research Laboratories
Office of Aerospace Research
United States Air Force
Bedford, Massachusetts

*This research was sponsored in part under Contract AF19(604)-8052 and in part by the Hughes Research Laboratories under the Howard Hughes Fellowship Program.

Light Scattering from Dielectric Film Laser Mirrors

Introduction:

Operation of the helium-neon gas-filled continuous wave laser at a wavelength of 6328Å, in the red, has permitted visual observation of the transverse mode pattern of the output beam, by placing a white card or ground glass screen in the beam. It is immediately apparent that the mode pattern is also visible on the mirror surfaces, by scattered light. This scattering of light from the cavity standing wave is an undesirable dissipation of the stored energy and reduces the cavity Q . The object of this work was to examine the mirror scattering from the point of view of laser operation.

Experiment:

The laser setup used was a helium and neon filled, direct current discharge tube, approximately centered in a cavity formed by a pair of one-meter radius mirrors, spaced 127 cm. apart. This is the configuration analyzed by Boyd and Gordon[1] and by Boyd and Kogelnik[2], and reported by Kogelnik and Rigrod[3]. The mirrors were quartz, with multilayer cryolite and zinc sulfide dielectric films, and were specially made to be highly reflective at the neon $3s_2$ to $2p_4$ transition line (6328Å). The laser cavity was stopped down to restrict the oscillation mode to a low order. Microscopic examination of the mirror surface by scattered light was made using a 50 power microscope. Photographs were taken with a microscope camera and adapter with an over-all magnification of 25 times.

ABSTRACT

The transverse mode pattern in a gas laser visible output beam can be seen on the dielectric film of the laser cavity mirrors; the eye is seeing light scattered by the film from the standing light wave in the cavity. This scattering results in a lowering of operating efficiency.

Microscopic examination of the scattered laser light shows that the light is scattered from small (2 to 20 microns) defects, covering about 4% of the mirror surface, and relatively widely spaced. The greater portion of the mirror surface has comparatively negligible scattering. Close correlation between the scattering of laser light and the scattering of white light permits a simple check for mirror scattering defects, by inspection under a medium power (about 50X) microscope.

The total loss of power due to absorption and scattering in the film is less than 1% of the cavity traveling wave power per transit. The effect of the scattering points on the laser beam itself are negligible.

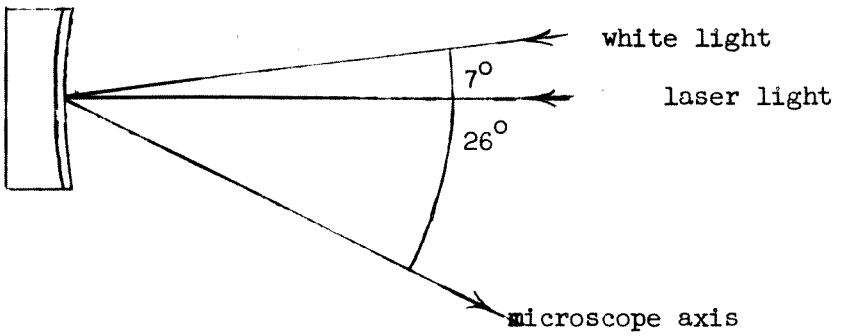

Photographs of the scattered light from the mirror surface are reproduced in Figures 1 and 2. Figure 1 was taken with only laser light incident, and Figure 2 was taken with only white light incident. Inspection of these photographs yields the following observations:

1. The laser transverse mode pattern is seen as a grouping of dots of scattered light into the characteristic mode pattern.
2. A relatively small percentage of the mirror surface area is taken up by the scattering points.
3. The scattering points, even after magnification, are very small.
4. Diffraction and interference effects appear on the right and left hand sides of the photographs.
5. The white light scattering points correlate closely with the laser light scattering points in location, in size and in intensity of scattered light.

Several dielectric film laser mirrors were examined for scattering points, with this result:

6. All the mirrors had scattering points in roughly the same density and size as the mirror photographed.

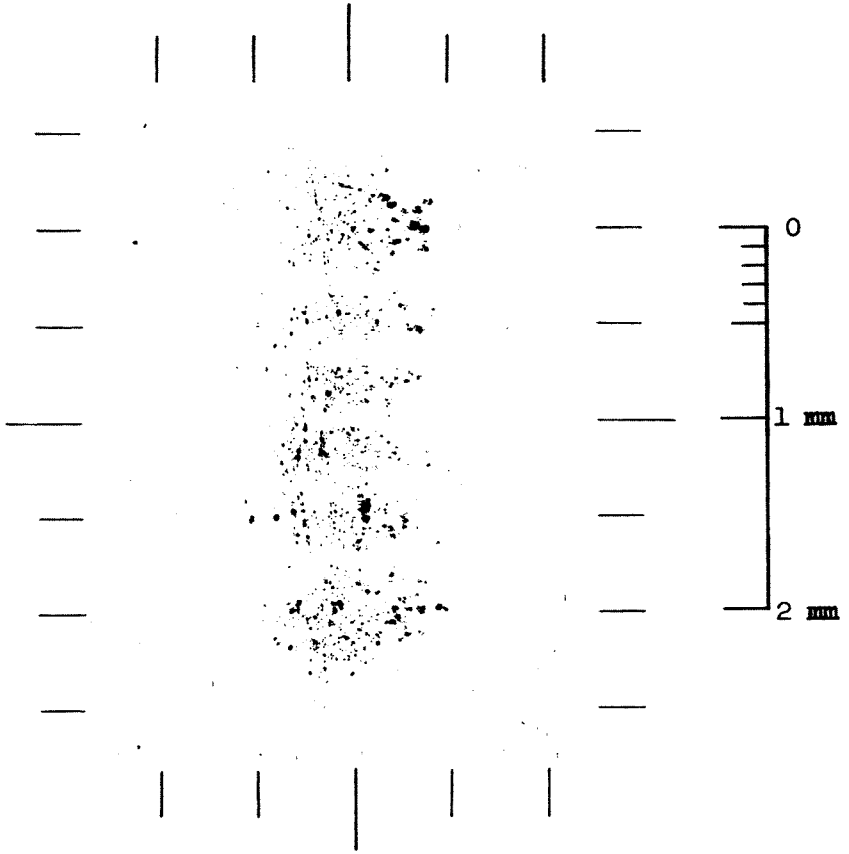

Figure 1

Laser light scattered from mirror surface, 25X magnification

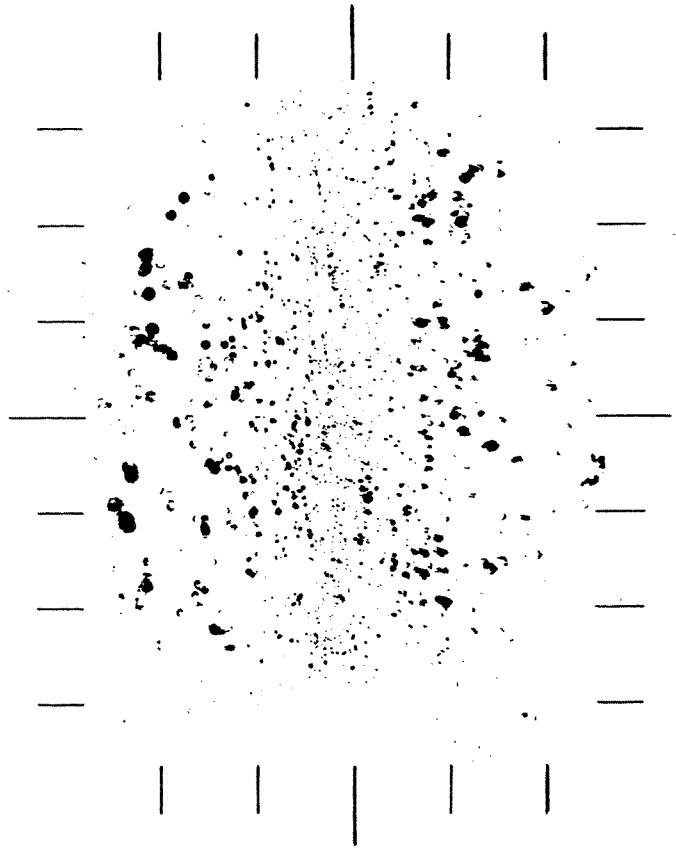

Figure 2

White light scattered from mirror surface, 25X magnification

A deposited gold film mirror also examined showed few scattering points.

Discussion:

A point by point discussion of the experimental results follows:

1. Figure 1 shows a TEM_{05} mode.
2. The smallness of the scattering area compared to the non-scattering area is an indication that the scattering points are, perhaps, avoidable defects.
3. An examination of the photograph of the scattering of a representative area of the dielectric film $\frac{1}{5} \times \frac{1}{5}$ mm square revealed 37 spots with an average diameter of 5 microns ranging from 2 to 20 microns, an average area of 44 square microns, and a total white area percentage of 4%. It is expected that this figure will be greater than the total scattering loss, since not all light incident on a scattering point is scattered, and possible over-exposure of the photographic film for a high-intensity scattering point will make it appear larger than it should. Polster[4] and Stone[5] report that the total loss from scattering and absorption in a typical multilayer dielectric film is less than 1% .
4. The mirror tangent plane having a dihedral angle of 26° with the microscope focal plane (line of intersection, vertical) combine with the small depth of field of the microscope at high magnifications to bring out Fresnel diffraction and interference patterns, where the microscope is not focused on the mirror surface. Focusing on the right or left edge of the mode pattern instead of the center shows about the same size and density of scattering points. The scattered white light shows Fresnel diffraction patterns also. This is due to the use of a projection lamp with a collimating lens as the white light source: measurements made on the cone of light passing through a pinhole show

that the cone of light incident on a point of the mirror surface was defined by a half-angle of 0.4° so that the noncoherent white light source still showed Fresnel diffraction and interference patterns, though not as distinctly.

5. The fact that the white light scattering points are the same as the monochromatic light scattering points rules out any special effect that might be attributable to the monochromaticity of the laser light. It also makes possible a check for mirror scattering points, consisting of a visual examination under a medium-power (50X) microscope, with white light.

6. Scattering points appear to be an unsolved problem in dielectric film techniques. Any change in the dielectric constant in a direction parallel to the mirror surface will scatter light from an incident beam. Possible explanations for the scattering points are:
   a) An uneven deposition rate, causing thin spots or pinholes in the thin layers.
   b) Disposition of relatively large chunks of the evaporated dielectric.
   c) Growth of crystals in the dielectric layer.

   Holland[6] discusses these problems, with others, in multilayer dielectric film technique.

Conclusion:

The transverse mode pattern in a gas laser visible output beam can be seen on the laser cavity mirrors; the eye is seeing light scattered by the mirror surface from the standing light wave in the cavity. This scattering results in a lowering of operating efficiency. Microscopic examination of the scattered laser light shows that the light is scattered from small (2 to 20 microns) defects covering about 4% of the mirror surface, and relatively widely spaced. The greater portion of the mirror

surface has comparatively negligible scattering. Close correlation between the scattering of laser light and the scattering of white light permits a simple check for mirror scattering defects, by inspection under a medium power (about 50X) microscope.

Because of the small size of the scattering points, and the small percentage of mirror surface area that they cover, the diffraction and interference effects of the light scattered into the laser beams are very small. The laser beam fills in its weak spots by diffraction, and its power is much greater than the power of the light scattered into the beam. For beam lengths greater than an inch or so, no effect of the scattering points on the beam is observable.

The largest effect of the scattering points is the reduction in standing wave energy storage. It will cause a loss of less than one percent of the cavity traveling wave power per transit.

REFERENCES

1. G. D. Boyd and J. P. Gordon, "Confocal Multi-mode Resonator for Millimeter through Optical Wavelength Masers", Bell Sys. Tech. Jour. 40, 489-508; March 1961.

2. G. D. Boyd and H. Kogelnik, "Generalized Confocal Resonator Theory", Bell Sys. Tech. Jour. 41, 1347-1369; July 1962.

3. H. Kogelnik and W. W. Rigrod, "Visual Display of Isolated Optical-Resonator Modes", Proc. IRE (correspondence) 50, 220; February 1962.

4. H. D. Polster, "A Symmetrical All-Dielectric Interference Filter", J. Opt. Soc. Am. 42, 21-24; January 1952.

5. J. M. Stone, "Refinements in the Preparation and Theory of Multilayer Films", J. Opt. Soc. Am. 43, 927-928; October 1953.

6. L. Holland, "Vacuum Deposition of Thin Films", John Wiley and Sons, Inc. New York, N.Y., pp. 294-297; 1956.

APPENDICES

PART II

APPENDIX E

INFINITE STRIP PLANE-PARALLEL MIRRORS RESONATOR EQUATION

Maxwell's equations for the electromagnetic field vectors in a source-free uniform dielectric medium are

$$\begin{aligned} \bar{\nabla} \times \bar{E} &= - j\omega\mu\bar{H} \\ \bar{\nabla} \times \bar{H} &= j\omega\epsilon\bar{E} \\ \bar{\nabla} \cdot \bar{E} &= 0 \\ \bar{\nabla} \cdot \bar{H} &= 0 \quad . \end{aligned} \tag{E.1}$$

Silver (68) uses the vector Green's theorem in the form

$$\int_v (\bar{F} \cdot \bar{\nabla} \times \bar{\nabla} \times \bar{G} - \bar{G} \cdot \bar{\nabla} \times \bar{\nabla} \times \bar{F})\, dv = - \int_{s_1+s_2+..+s_n} (\bar{G} \times \bar{\nabla} \times \bar{F} - \bar{F} \times \bar{\nabla} \times \bar{G}) \cdot \bar{n}\, ds \tag{E.2}$$

where $\bar{F}$ and $\bar{G}$ are two continuous vector functions of position in the volume v with boundary surfaces $s_1 + s_2 + \ldots + s_n$, and $\bar{n}$ is the unit vector normal to s directed into v. By letting $\bar{G}$ be the vector function

$$\bar{G} = \bar{a}\,\psi = \bar{a}\,\frac{e^{-jkr}}{r} \quad , \qquad \text{E.3}$$

where $\bar{a}$ is an arbitrary constant vector and r is the magnitude of the radius vector $\bar{r}$ from the field point to the source point, and letting $\bar{F}$ become $\bar{E}$ or $\bar{H}$, suitable transformations of Eq. E.2 yield

$$\bar{E}_P = \frac{1}{4\pi} \int_{s_1+s_2+..+s_n} [-j\omega\mu\,\psi\,(\bar{n} \times \bar{H}) + (\bar{n} \times \bar{E}) \times \bar{\nabla}\,\psi + (\bar{n} \cdot \bar{E})\,\bar{\nabla}\,\psi]\,ds$$

$$\bar{H}_P = \frac{1}{4\pi} \int_{s_1+s_2+..+s_n} [j\omega\epsilon\,\psi\,(\bar{n} \times \bar{E}) + (\bar{n} \times \bar{H}) \times \bar{\nabla}\,\psi + (\bar{n} \cdot \bar{H})\,\bar{\nabla}\,\psi]\,ds \qquad \text{E.4}$$

where $\bar{E}_P$ and $\bar{H}_P$ are the electromagnetic field vectors at the point P in volume v due to the sources within the surfaces s_i, their effect taken into account through the fields that they produce on the surfaces s_i.

These equations are the analytic formulation of the Huyghens-Fresnel principle, which states that each point on a given wavefront s can be regarded as a secondary source which gives rise to a spherical wavelet, and that the wave at a field point P is to be obtained by superposition of these elementary wavelets, with due regard to their phase differences when they arrive at the point P.

By adding a surface integral of value zero, Eq. E.4 can be converted to (69)

$$\bar{E}_P = -\frac{1}{4\pi}\int_S \left(\psi \frac{\partial \bar{E}}{\partial n} - \bar{E}\frac{\partial \psi}{\partial n}\right)$$

$$\bar{H}_P = -\frac{1}{4\pi}\int_S \left(\psi \frac{\partial \bar{H}}{\partial n} - \bar{H}\frac{\partial \psi}{\partial n}\right) \qquad \text{E.5}$$

where

$$\frac{\partial \psi}{\partial n} = (\bar{\nabla}\,\psi)\cdot\bar{n} \quad . \qquad \text{E.6}$$

If the electromagnetic field vectors are written in Cartesian coordinates, then each of the components of $\bar{E}_P$ and $\bar{H}_P$ separately satisfies the equation

$$u_P = -\frac{1}{4\pi}\int_S \left(\psi \frac{\partial u}{\partial n} - u\frac{\partial \psi}{\partial n}\right) \quad . \qquad \text{E.7}$$

By writing out $\partial\psi/\partial n$ from Eq. E.6, Eq. E.7 becomes

$$u_P = -\frac{1}{4\pi}\int_S \frac{e^{-jkr}}{r}\left[u\left(jk + \frac{1}{r}\right)\cos(\bar{n},\bar{r}) + \frac{\partial u}{\partial n}\right] ds \quad . \qquad \text{E.8}$$

For the optical resonators of interest, the field can be taken approximately as a plane wave, so that only one component of $\bar{E}$ and $\bar{H}$ is needed, satisfying Eq. E.8. The assumed planar wave permits the approximation

$$\frac{\partial u}{\partial n} \approx -jku \quad . \qquad \text{E.9}$$

For the plane-parallel mirrors, $\bar{n} = \bar{e}_z$ and a mirror separation d yield

$$\cos(\bar{n},\bar{r}) = -\frac{d}{r} \quad . \tag{E.10}$$

Equation E.8 becomes

$$u_P = -\frac{1}{4\pi}\int_s \frac{e^{-jkr}}{r}\, u\left(-j\,\frac{kd}{r} - \frac{d}{r^2} - jk\right) ds \tag{E.11}$$

which for

$$kd \gg 1 \quad , \tag{E.12}$$

reduces to

$$u_P = \frac{jk}{4\pi}\int_s \frac{e^{-jkr}}{r}\, u\left(1 + \frac{d}{r}\right) ds \quad . \tag{E.13}$$

For the case of an infinite strip resonator of half width b, with no variation with the y coordinate (along the slit), Eq. E.13 becomes

$$u_P(x_2) = \frac{jk}{4\pi}\int_{x_1=-b}^{b} dx_1 \int_{y_1=-\infty}^{\infty} dy_1\, \frac{e^{-jkr}}{r}\, u(x_1)\left(1 + \frac{d}{r}\right) \tag{E.14}$$

with

$$r = \left[(x_2 - x_1)^2 + y_1^{\,2} + d^2\right]^{\frac{1}{2}} \quad . \tag{E.15}$$

The integration over y_1 can be performed by the method of stationary phase (70), since k is much greater than one. In the integrand r can be set equal to

$$\rho = [d^2 + (x_2 - x_1)^2]^{\frac{1}{2}} \qquad \text{E.16}$$

except in the argument of the exponential. The result of the method of stationary phase integration on the exponential is

$$\int_{-\infty}^{\infty} dy \exp[-ik(\rho^2 + y^2)^{\frac{1}{2}}] \approx (\lambda/j\rho)^{\frac{1}{2}} (1 + d/\rho) \exp(-ik\rho) \qquad \text{E.17}$$

so that Eq. E.14 becomes

$$u_p(x_2) = \tfrac{1}{2} (j/\lambda)^{\frac{1}{2}} \int_{x_1=-b}^{b} dx_1 \frac{\exp(-jk\rho)}{\sqrt{\rho}} (1 + \frac{d}{\rho}) u(x_1) \ . \qquad \text{E.18}$$

When the resonator dimensions satisfy the conditions

$$\begin{aligned} b^2/\lambda d &\ll (d/b)^2 \\ 4\, b^2/d^2 &\ll 1 \ , \end{aligned} \qquad \text{E.19}$$

ρ can be set equal to d in the denominator, and set to

$$\rho \approx d + (x_2 - x_1)^2/2d \qquad \text{E.20}$$

in the exponent, yielding, for P a point on mirror two,

$$u_2(x_2) = (\lambda d)^{-\frac{1}{2}} \exp[j(\pi/4 - kd)] \cdot \cdot \int_{-b}^{b} dx_1 \exp[-jk(x_2 - x_1)^2/2d]\, u_1(x_1) \ . \qquad \text{E.21}$$

APPENDIX F

METHOD OF CALCULATION AND COMPUTER PROGRAMS FOR MASKED MIRRORS EQUATION

The methods used to solve the matrix eigenvalue equation for the dominant mode eigenvector and eigenvalue are the Von Mises, or power, iteration method (71,72), and the Rayleigh-Aitken quotient (73,74).

The eigenvalue problem we wish to solve is

$$A\, x_i = \lambda_i\, x_i \qquad \text{F.1}$$

where x_i , $i = 1, 2, \ldots n$, are the n orthonormal eigenvectors associated with the n eigenvalues λ_i in the n-dimensional space of the matrix A . The eigenvalue of largest amplitude, the one for the dominant mode, is chosen to be λ_1 .

The power iteration method starts with an arbitrary initial vector v given by

$$v = \sum_{i=1}^{n} \beta_i\, x_i \quad , \qquad \text{F.2}$$

where β_1 is, if possible, chosen to be large compared to all others. Multiplying v by A gives

$$v_1 = A\, v = \sum_{i=1}^{n} \beta_i\, \lambda_i\, x_i \quad . \qquad \text{F.3}$$

This can be written

$$v_1 = \lambda_1 \sum_{i=1}^{n} \beta_i \, (\lambda_i/\lambda_1) \, x_i \quad . \qquad \text{F.4}$$

Multiplying again by A gives

$$v_2 = A \, v_1 = \lambda_1^{\,2} \sum_{i=1}^{n} \beta_i \, (\lambda_i/\lambda_1)^2 \, x_i \qquad \text{F.5}$$

and, for s multiplications,

$$v_s = \lambda_1^{\,s} \sum_{i=1}^{n} \beta_i \, (\lambda_i/\lambda_1)^s \, x_i \quad . \qquad \text{F.6}$$

If s is taken sufficiently large, the magnitude of all other components can be made as small relative to the component of x_1 as is desired. Then the vector v_s is a multiple of the eigenvector. The eigenvalue is given by

$$\lambda_1 = v_{s+1}/v_s \quad . \qquad \text{F.7}$$

Provision to handle the case of $|\lambda_1| = |\lambda_2| > \ldots$ is built into the eigenvalue problem solution subroutine, but it was not needed.

The Rayleigh-Aitkens quotient evaluates the eigenvalue by forming two sequences,

$$\begin{aligned} v_s &= A^s \, v \quad , \\ \omega'_t &= \omega' \, A^t \end{aligned} \qquad \text{F.8}$$

where the prime indicates the transpose of a vector. As s and t

increase, v_s converges linearly to the eigencolumn x_1 and ω'_t converges to the eigenrow v_1, corresponding to λ_1. The scalar product

$$\omega'_m v_k = \omega' A^{k+m} v \qquad \text{F.9}$$

becomes

$$\omega' A^{k+m} v = \omega' X D^{k+m} X^{-1} v \qquad \text{F.10}$$

where D is the matrix of the eigenvalues and X is the matrix such that

$$A X = X D \quad . \qquad \text{F.11}$$

Equation F.10 is a polynomial of degree $k + m$ in the λ_i's. The quotients

$$\lambda_1 = \omega'_{m+1} v_k / \omega'_m v_k$$

$$\lambda_1 = \omega'_m v_{k+1} / \omega'_m v_k \qquad \text{F.12}$$

give a better result for λ_1 than does Eq. F.7.

The Fortran IV programs written for use with the IBM 7094 to carry out the procedures outlined above are reproduced on the following pages.

The SLF deck is the main program, in which the parameters are read in, the kernel is calculated, and all data writing is done.

The EIGCM deck solves the complex matrix eigenvalue problem.

The CMVMUL deck performs complex matrix times complex vector multiplications.

The CSPV deck performs complex vector scalar product multiplications.

The RITOAP deck converts a complex vector in real and imaginary parts form to an amplitude and phase in degrees form.

The NORMAL deck converts a complex vector to an amplitude and phase in degrees form, normalized to the component of largest amplitude.

```
$IBFTC SLF     DECK
      COMPLEX K,CEXP,LAMBDA,EVAL1,EVAL2,EIGV1,EIGV2,AP,Z0,Z1,Z2,V0,V1,V2
      DIMENSION K(50,50),AP(50,50),Z0(50),Z1(50),Z2(50),V0(50),V1(50),
     1 V2(50)
      DIMENSION ISYM(2),ETA(50),Y1(50),Y2(50)
      DIMENSION EIGV1(50),EIGV2(50)
      DATA ISYM(1),ISYM(2) /4HEVEN,3HODD/
      DATA PI/3.1415926/
      PLOSS(X) = 100.0 * (1.0 - (X * PLF) ** 2)
      PHASH(X) = 45.0 + X
   10 READ (5,500) N, ALPHA, BETA
      SCALE = (1.0 - ALPHA) / (FLOAT(N) - 1.0)
      PLF = BETA * SCALE
      PIBETA = PI * (BETA*BETA)
      SIGN = 1.0
      ISET = ISYM(1)
   15 DO 30 I = 1, N
      CI = I - 1
      XSIR = ALPHA + CI * SCALE
      ETA(I) = XSIR
      DO 25 J = 1, N
      CJ = J - 1
      ZS = ALPHA + CJ * SCALE
      K(I,J) = CEXP((0.0,-1.0)*PIBETA*(ZS-XSIR)*(ZS-XSIR))
     1 + SIGN * CEXP((0.0,-1.0)*PIBETA*(ZS+XSIR)*(ZS+XSIR))
   25 CONTINUE
   30 CONTINUE
      DO 40 I = 1,N
      K(I,1) = .5 * K(I,1)
      K(I,N) = .5 * K(I,N)
   40 CONTINUE
      CALL EIGCM(N,K,EVAL1,EVAL2,EIGV1,EIGV2,NUMBER,AP,Z0,Z1,
     1 Z2,V0,V1,V2)
      WRITE (6,512) ISET,N,ALPHA,BETA
      L = NUMBER + 1
      GO TO (100,70,80), L
   70 CALL RITOAP(1,EVAL1,EVAL1)
      CALL NORMAL(N,EIGV1,EIGV1,EIGV1,JLARG)
      WRITE (6,510) EVAL1,EIGV1
      A = PLOSS(REAL(EVAL1))
      B = PHASH(AIMAG(EVAL1))
      WRITE (6,530) A,B
      DO 73 I = 1,N
      Y1(I) = REAL(EIGV1(I))
      Y2(I) = AIMAG(EIGV1(I))
   73 CONTINUE
      CALL XYPLOT(50,ETA,Y1,+0.0,+2.5,+0.0,+1.25,DD,0)
      CALL XYPLOT(50,ETA,Y2,-1.5,+1.0,-60.0,+40.0,DD,1)
      GO TO 75
   80 CALL RITOAP(1,EVAL1,EVAL1)
      CALL NORMAL(N,EIGV1,EIGV1,EIGV1,JLARG)
      WRITE (6,510) EVAL1,EIGV1
      A = PLOSS(REAL(EVAL1))
      B = PHASH(AIMAG(EVAL1))
      WRITE (6,530) A,B
      DO 83 I = 1,N
      Y1(I) = REAL(EIGV1(I))
      Y2(I) = AIMAG(EIGV1(I))
   83 CONTINUE
      CALL XYPLOT(50,ETA,Y1,+0.0,+2.5,+0.0,+1.25,DD,0)
```

```
      CALL XYPLOT(50,ETA,Y2,-1.5,+1.0,-60.0,+40.0,DD,1)
      CALL RITOAP(1,EVAL2,EVAL2)
      CALL NORMAL(N,EIGV2,EIGV2,EIGV2,JLARG)
      WRITE (6,511) EVAL2,EIGV2
      A = PLOSS(REAL(EVAL2))
      B = PHASH(AIMAG(EVAL2))
      WRITE (6,530) A,B
      DO 95 I = 1,N
      Y1(I) = REAL(EIGV2(I))
      Y2(I) = AIMAG(EIGV2(I))
   95 CONTINUE
      CALL XYPLOT(50,ETA,Y1,+0.0,+2.5,+0.0,+1.25,DD,0)
      CALL XYPLOT(50,ETA,Y2,-1.5,+1.0,-60.0,+40.0,DD,1)
   75 IF(SIGN .LT. 0.0) GO TO 10
      SIGN = - 1.0
      ISET = ISYM(2)
      GO TO 15
  100 WRITE (6,520)
      STOP
  500 FORMAT(I5,2F10.4)
  510 FORMAT(/1X 13HEIGENVALUE = 2E15.8, 10X13HEIGENVECTOR = 2E15.8,
     1/(67X2E15.8))
  511 FORMAT(/1X18H2ND EIGENVALUE =  2E15.8,10X13HEIGENVECTOR = 2E15.8,
     1 /(72X2E15.8))
  512 FORMAT(1H1 10XA6,2X8HSYMMETRY,5X4HN = I5,5X8HALPHA = F10.4,5X
     1 7HBETA = F10.4//)
  520 FORMAT(1H111HNO SOLUTION  /)
 5300FORMAT ( // 5X33HPERCENT POWER LOSS PER TRANSIT = F10.5,15X34HDEGR
     1EES PHASE SHIFT PER TRANSIT = F10.5)
       END
```

```
$IBFTC NORMAL  DECK
C      THIS SUBROUTINE CALLS SUBROUTINE RITOAP TO CONVERT A COMPLEX
C      VECTOR COMPLX IN REAL,IMAG TO A COMPLEX VECTOR CONVRT IN
C      AMPPHADEG, AND NORMALIZES IT TO THE JLARGETH COMPONENT HAVING THE
C      LARGEST MAGNITUDE IN A COMPLEX VECTOR NORMLI IN AMPPHADEG.
C      DIMENSION = DIMEN.  COMPLX = CONVRT = NORMLI IS POSSIBLE
       SUBROUTINE NORMAL(DIMEN,COMPLX,CONVRT,NORMLI,JLARGE)
       COMPLEX COMPLX(DIMEN),CONVRT(DIMEN),NORMLI(DIMEN)
       INTEGER DIMEN
       CALL RITOAP(DIMEN,COMPLX,CONVRT)
       JLARGE = 1
       A = REAL(CONVRT(1))
       DO 1 J = 2,DIMEN
       IF (REAL(CONVRT(J)).LT.A) GO TO 1
       JLARGE = J
       A = REAL(CONVRT(J))
     1 CONTINUE
       P = AIMAG(CONVRT(JLARGE))
       DO 2 J = 1,DIMEN
       AMP = REAL(CONVRT(J)) / A
       PHA = AIMAG(CONVRT(J)) - P
     2 NORMLI(J) = CMPLX(AMP,PHA)
       RETURN
        END
```

```
$IBFTC EIG      DECK
C       GREATEST EIGENVALUE(S) WITH EIGENVECTOR(S) FOR NONSYMMETRICAL COM-KWJ  S21
C       PLEX MATRIX  (V.MISES ITERATION AND RAYLEIGH QUOTIENT)            KWJ  S21
        SUBROUTINE EIGCM (M,A,LA1,LA2,EIGV1,EIGV2,NUMB,AP,Z0,Z1,Z2,V0,V1,
       1 V2)
        DIMENSION A(50,M),EIGV1(M),EIGV2(M),Z0(M),Z1(M),Z2(M),V0(M),V1(M) KWJ  S21
       1,V2(M),AP(50,M)                                                   KWJ  S21
        COMPLEX A,EIGV1,EIGV2,Z0,Z1,Z2,V0,V1,V2,LA1,LA2,K1,K2,K3,K4,       KWJ  S21
       1A0,A1,D,LAPR,A0PR,AP,CSQ
        DO 10 I = 1, M                                                    KWJ  S21
        Z2(I) = (1.,0.)
    10  V2(I) = (1.,0.)
        K4 = FLOAT(M) * (1.,0.)                                           KWJ  S21
        A0PR = (0.,0.)                                                    KWJ  S21
        LAPR = (0.,0.)                                                    KWJ  S21
        IC = 2                                                            KWJ  S21
        IS = 0                                                            KWJ  S21
        ID = 0                                                            KWJ  S21
        DO 20 I = 1, M                                                    KWJ  S21
        DO 20 K = 1, M                                                    KWJ  S21
    20  AP(K,I) = A(I,K)                                                  KWJ  S21
    30  IF(IC .GT. 50) GO TO 100                                          KWJ  S21
        CSQ = CSQRT(K4)                                                   KWJ  S21
        DO 32 J = 1, M                                                    KWJ  S21
        Z0(J) = Z2(J) / CSQ                                               KWJ  S21
    32  V0(J) = V2(J) / CSQ                                               KWJ  S21
        CALL CMVMUL(M,A,Z0,Z1)                                            KWJ  S21
        CALL CMVMUL(M,A,Z1,Z2)                                            KWJ  S21
        CALL CMVMUL(M,AP,V0,V1)                                           KWJ  S21
        CALL CMVMUL(M,AP,V1,V2)                                           KWJ  S21
        CALL CSPV(M,V0,Z1,K1)                                             KWJ  S21
        CALL CSPV(M,V0,Z2,K2)                                             KWJ  S21
        CALL CSPV(M,V1,Z2,K3)                                             KWJ  S21
        CALL CSPV(M,V2,Z2,K4)                                             KWJ  S21
        LA1 = K4 / K3                                                     KWJ  S21
        D = K2 - K1**2                                                    KWJ  S21
        IC = IC + 2                                                       KWJ  S21
        IF(REAL(CABS(D/K2)) -1.E-6) 40,40,50
    40  ID = 0                                                            KWJ  S21
        IF(REAL(CABS((LA1-LAPR)/LA1)) .GT. 1.E-6)  IS=IS - 1
        IS = IS + 1                                                       KWJ  S21
        LAPR = LA1                                                        KWJ  S21
        IF(IS .EQ. 2) GO TO 110                                           KWJ  S21
        GO TO 30                                                          KWJ  S21
    50  IS = 0                                                            KWJ  S21
        A0 = (K1*K3-K2**2) / D                                            KWJ  S21
        IF(REAL(CABS((A0-A0PR)/A0)) .GT. 1.E-6)   ID=ID-1
        ID = ID + 1                                                       KWJ  S21
        A0PR = A0                                                         KWJ  S21
        IF(ID .EQ. 2) GO TO 120                                           KWJ  S21
        GO TO 30                                                          KWJ  S21
   100  NUMB = 0                                                          KWJ  S21
        RETURN                                                            KWJ  S21
   110  NUMB = 1                                                          KWJ  S21
        DO 112 L = 1, M                                                   KWJ  S21
        EIGV1(L) = Z0(L)                                                  KWJ  S21
   112  EIGV2(L) = (0.,0.)                                                KWJ  S21
        LA2 = (0.,0.)                                                     KWJ  S21
        RETURN                                                            KWJ  S21
   120  NUMB = 2                                                          KWJ  S21
```

```
      A1 = (K1*K2-K3) / D                                              KWJ  S21
      K1 = CSQRT(.25*A1**2-A0)                                         KWJ  S21
      LA1 = - A1 * .5 + K1                                             KWJ  S21
      LA2 = - A1 * .5 - K1                                             KWJ  S21
      DO 122 L = 1, M                                                  KWJ  S21
      EIGV1(L) = Z2(L) - LA2 * Z1(L)                                   KWJ  S21
  122 EIGV2(L) = Z2(L) - LA1 * Z1(L)                                   KWJ  S21
      RETURN                                                           KWJ  S21
       END                                                             KWJ  S21
```

```
$IBFTC CMV      DECK
C       MATRIX - VECTOR - MULTIPLICATION(COMPLEX), A * X = Y           KWJ  S19
        SUBROUTINE CMVMUL(N,A,X,Y)                                     KWJ  S19
        DIMENSION A(50,N), X(N), Y(N)                                  KWJ  S19
        COMPLEX A, X, Y                                                KWJ  S19
        DO 10 I = 1, N                                                 KWJ  S19
        Y(I) = (0.,0.)                                                 KWJ  S19
        DO 10 J = 1, N                                                 KWJ  S19
     10 Y(I) = Y(I) + X(J) * A(I,J)                                    KWJ  S19
        RETURN                                                         KWJ  S19
         END                                                           KWJ  S19
```

```
$IBFTC CSP      DECK
C       SCALAR PRODUCT OF VECTORS (COMPLEX), XP * Y = C                KWJ  S20
        SUBROUTINE CSPV(N,XP,Y,C)                                      KWJ  S20
        DIMENSION XP(N), Y(N)                                          KWJ  S20
        COMPLEX XP, Y, C                                               KWJ  S20
        C = (0.,0.)                                                    KWJ  S20
        DO 10 I = 1, N                                                 KWJ  S20
     10 C = C + XP(I) * Y(I)                                           KWJ  S20
        RETURN                                                         KWJ  S20
         END                                                           KWJ  S20
```

```
$IBFTC RITOAP  DECK
C       THIS SUBROUTINE CONVERTS A COMPLEX LINEAR ARRAY, COMPLX(DIMENS),
C       IN REAL - IMAGINARY FORM, TO A COMPLEX LINEAR ARRAY,
C       CONVRT(DIMENS), IN AMPLITUDE - PHASE IN DEGREES FORM
C       COMPLX = CONVRT IS POSSIBLE
        SUBROUTINE RITOAP(DIMENS,COMPLX,CONVRT)
        INTEGER DIMENS
        COMPLEX COMPLX(DIMENS),CONVRT(DIMENS)
        DO 20001 I = 1,DIMENS
        AMPLIT = SQRT(REAL(COMPLX(I)) ** 2 + AIMAG(COMPLX(I)) ** 2)
        PHASE  = ATAN(AIMAG(COMPLX(I)) / REAL(COMPLX(I))) * 57.29578
20001 CONVRT(I) = CMPLX(AMPLIT,PHASE)
        RETURN
         END
```

REFERENCES

1. A. L. Schawlow and C. H. Townes, "Infrared and Optical Masers", Phys. Rev. 112, 1940 (1958).

2. A. M. Prokhorov, "Molecular Amplifier and Generator for Submillimeter Waves", Soviet Physics JETP 7, 1140 (1958).

3. R. H. Dicke, U. S. Patent No. 2,851,652 (1958).

4. A. G. Fox and T. Li, "Resonant Modes in a Maser Interferometer", Bell System Tech. J. 40, 453 (1961).

5. P. Connes, "Augmentation du Produit Luminosité x Résolution des Interférometres par L'Emploi d'une Différence des Marches Indépendante de L'Incidence", Revue d'Optique 35, 37 (1956).

6. P. Connes, "L'Etalon de Fabry-Perot Spherique", J. Phys. Radium 19, 261 (1958).

7. G. D. Boyd and J. P. Gordon, "Confocal Multimode Resonator for Millimeter through Optical Wavelength Masers", Bell System Tech. J. 40, 489 (1961).

8. G. D. Boyd and H. Kogelnik, "Generalized Confocal Resonator Theory", Bell System Tech. J. 41, 1347 (1962).

9. G. Goubau and F. Schwering, "On the Guided Propagation of Electromagnetic Wave Beams", IRE Trans. on Antennas and Propagation AP-9, 248 (1961).

10. A. G. Fox and T. Li, "Modes in a Maser Interferometer with Curved and Tilted Mirrors", Proc. IEEE 51, 80 (1963).

11. A. G. Fox and T. Li, "Modes in a Maser Interferometer With Curved Mirrors", in Proceedings of the Third International Conference on Quantum Electronics (Columbia University Press, New York, 1964), Vol. 2, p. 1268.

12. R. F. Soohoo, "Nonconfocal Multimode Resonator for Masers", Proc. IEEE 51, 70 (1963).

13. C. Y. She and H. Heffner, "Analysis of Spherical Sector Resonators for the Production of a Focused Laser Beam", Appl. Opt. 3, 703 (1964).

14. L. Bergstein and H. Schachter, "Resonant Modes of Optic Interferometer Cavities. I. Plane-Parallel End Reflectors", J. Opt. Soc. Am. 54, 887 (1964).

15. D. E. McCumber, "Eigenmodes of a Symmetric Cylindrical Confocal Laser Resonator and their Perturbation by Output-Coupling Apertures", Bell System Tech. J. 44, 333 (1965).

16. J. Kotik and M. C. Newstein, "Theory of Laser Oscillations in Fabry-Perot Resonators", J. Appl. Phys. 32, 178 (1961).

17. S. R. Barone, "Resonances of the Fabry-Perot Resonator", J. Appl. Phys. 34, 831 (1963).

18. L. A. Vaĭnshteĭn, "Open Resonators for Lasers", Soviet Physics JETP 17, 709 (1963).

19. L. A. Vaĭnshteĭn, "Open Resonators with Spherical Mirrors", Soviet Physics JETP 18, 471 (1964).

20. L. A. Vaĭnshteĭn, "Diffraction in Open Resonators and Open Waveguides with Plane Mirrors", Soviet Physics JETP 9, 157 (1964).

21. L. A. Vaĭnshteĭn, "Open Resonators with Cylindrical Mirrors", Soviet Physics JETP 9, 166 (1964).

22. P. O. Clark, "An Analysis of Multireflector Optical Resonators", Ph.D. dissertation, California Institute of Technology, 1964.

23. J. F. Asmus, "An Analysis of Perturbed Confocal Resonators", Ph.D. dissertation, California Institute of Technology, 1965.

24. H. Kogelnik and W. W. Rigrod, "Visual Display of Isolated Optical-Resonator Modes", Proc. IRE 50, 220 (1962).

25. T. G. Polyani and W. R. Watson, "Gaseous Optical Maser with External Mirrors", J. Appl. Phys. 34, 553 (1963).

26. W. R. Watson and T. G. Polyani, "Radiation Patterns of Confocal He-Ne Laser", J. Appl. Phys. 34, 708 (1963).

27. P. M. Morse and H. Feshbach, "Methods of Theoretical Physics", McGraw-Hill Book Company, Inc., New York, 1953; Vol. II, Chap. 13, pp. 1764-1767.

28. C. Flammer, "The Vector Wave Function Solution of the Diffraction of Electromagnetic Waves by Circular Disks and Apertures. I. Oblate Spheroidal Vector Wave Functions", J. Appl. Phys. 24, 1218 (1953).

29. R. W. Zimmerer, "Spherical Mirror Fabry-Perot Resonators", IEEE Trans. on Microwave Theory and Techniques MTT-11, 371 (1963).

30. M. Ito, "Transmitter for Coherent Light Communication System", presented at the IEEE International Convention, New York, March 1964.

31. C. Flammer, "Spheroidal Wave Functions", Stanford University Press, Stanford, California, 1957.

32. See Ref. 27, Chap. 11, pp. 1502-1513.

33. J. A. Stratton, "Electromagnetic Theory", McGraw-Hill Book Company, Inc., New York, 1941; Chap. VII, pp. 420-421.

34. J. A. Stratton, P. M. Morse, L. J. Chu, J. D. C. Little, and F. J. Corbató, "Spheroidal Wave Functions", John Wiley and Sons, Inc., New York, 1956.

35. A. Leitner and R. D. Spence, "The Oblate Spheroidal Wave Functions" J. Franklin Inst. 249, 299 (1950).

36. J. Meixner and F. W. Schäfke, "Mathieusche Funktionen und Spharoidfunktionen", Springer-Verlag, Berlin, 1954.

37. M. Abramowitz and I. A. Stegun, "Handbook of Mathematical Functions", Applied Mathematics Series No. 55, National Bureau of Standards, U. S. Department of Commerce, 1964.

38. E. Pinney, "Laguerre Functions in the Mathematical Foundations of the Electromagnetic Theory of the Paraboloid Reflector", J. Math. Phys. 25, 49 (1946).

39. W. Magnus and F. Oberhettinger, "Formulas and Theorems for the Functions of Mathematical Physics", Chelsea Publishing Company, New York, 1954.

40. E. Jahnke and F. Emde and F. Lösch, "Tables of Higher Functions", McGraw-Hill Book Company, Inc., New York, 1960; Sixth edition, p. 98.

41. W. W. Rigrod, "Isolation of Axi-Symmetrical Optical-Resonator Modes", in Proceedings of the Third International Conference on Quantum Electronics (Columbia University Press, New York, (1964), Vol. 2, p. 1285; and Appl. Phys. Ltrs. 2, 51 (1963).

42. M. Abraham,"Elektrische Schwingungen in einem frei endigen Draht", Ann. Physik 2, 32 (1900).

43. L. Page and N. I. Adams, "The Electrical Oscillations of a Prolate Spheroid. Paper I", Phys. Rev. 53, 819 (1938).

44. R. M. Ryder, "The Electrical Oscillations of a Perfectly Conducting Prolate Spheroid", Ph.D. dissertation, Yale University, 1940; and J. Appl. Phys. 13, 327 (1942).

45. L. J. Chu and J. A. Stratton, "Steady-State Solutions of Electromagnetic Field Problems. III. Forced Oscillations of a Prolate Spheroid", J. Appl. Phys. 12, 241 (1941).

46. J. C. Simons, "Electromagnetic Resonant Behavior of a Confocal Spheroidal Cavity System in the Microwave Region", Ph.D. dissertation, Massachusetts Institute of Technology, 1950.

47. A. Leitner and R. D. Spence, "Effect of a Circular Groundplane on Antenna Radiation", J. Appl. Phys. 21, 1001 (1950).

48. T. Nimura, "Resonance Frequency of Spheroidal Cavity Resonator", Sci. Rep. Res. Inst. Tohoku University, The Research Institute of Electrical Communication, vol. 1/2, 73 (1951).

49. E. C. Hatcher and A. Leitner, "Radiation from a Point Dipole Located at the Tip of a Prolate Spheroid", J. Appl. Phys. 25, 1250 (1954).

50. See Ref. 33, pp. 422-423.

51. W. Culshaw, "Further Considerations on Fabry-Perot Type Resonators", IRE Trans. on Microwave Theory and Techniques MTT-10, 331 (1962).

52. A. Yariv and J. P. Gordon, "The Laser", Proc. IEEE 51, 4 (1963).

53. W. R. Smythe, "Static and Dynamic Electricity", McGraw-Hill Book Company, Inc., New York, 1950; Chap. 13, pp. 441-442.

54. See Ref. 53, Chap. 11, pp. 391-392.

55. D. L. Perry, "Low Loss Multilayer Dielectric Mirrors", presented at the Northeast Electronics Research and Engineering Meeting, November 1964.

56. O. S. Heavens, "Optical Properties of Thin Solid Films", Academic Press Inc., New York, 1955.

57. J. B. Beier and E. H. Scheibe, "Higher Modes in Guided Electromagnetic-Wave Beams", IRE Trans. on Antennas and Propagation AP-10, 349 (1962).

58. J. N. Franklin, "Computation of Eigenvalues by the Method of Iteration", California Institute of Technology Computing Center Technical Report No. 111, October 1957.

59. E. Bodewig, "Matrix Calculus", Interscience Publishers, Inc., New York, 1959; p. 292.

60. J. P. Gordon and H. Kogelnik, "Equivalence Relations among Spherical Mirror Optical Resonators", Bell System Tech. J. 43, 2873 (1964).

61. V. Evtuhov and J. K. Neeland, Twenty-first Annual Conference on Electron Device Research, June 1963 (unpublished).

62. V. Evtuhov and J. K. Neeland, "Pulsed Ruby Lasers", Hughes Research Laboratories Research Report No. 309, August 1964, pp. 102-106.

63. V. Evtuhov and J. K. Neeland, private communication.

64. Y. Suematsu and K. Iga, "Experiment on Quasi-Fundamental Mode Oscillation of Ruby Laser", IEEE 52, 87 (1964).

65. A. E. Siegman, "Small-Mirror Transverse-Mode Control and Near-Field Rings in Ruby-Laser Rods", J. Opt. Soc. Am. 54, 567 (1964), Abstract TB 14, presented at the Meeting of the American Optical Society, Spring 1964.

66. C. K. N. Patel, W. L. Faust, R. A. McFarlane, and C. G. B. Garrett, "Laser Action up to 57.355μ in Gaseous Discharges (Ne, He-Ne)", Appl. Phys. Ltrs. 4, 18 (1964).

67. J. T. LaTourette, S. F. Jacobs, and P. Rabinowitz, "Improved Laser Angular Brightness Through Diffraction Coupling", Appl. Opt. 3, 981 (1964).

68. S. Silver, "Microwave Antenna Theory and Design", Massachusetts Institute of Technology Radiation Laboratory Series, Vol. 12, McGraw-Hill Book Company, Inc., New York, 1949.

69. B. B. Baker and E. T. Copson, "The Mathematical Theory of Huygens' Principle", Oxford, The Clarendon press, 1939.

70. J. Mathews and R. L. Walker, "Methods of Mathematical Physics", W. A. Benjamin, Inc., New York, 1964; p. 85.

71. See Ref. 59, pp. 269-287.

72. R. Zurmühl, "Praktische Mathematik für Ingenieure und Physiker", Springer-Verlag, Berlin, Fourth Edition, 1963.

73. See Ref. 59, p. 283.

74. See Ref. 72, pp. 163-177.

75. G. E. Deschamps and P. E. Mast, "Beam Tracing and Applications", in the Proceedings of the Symposium on Quasi-Optics, Microwave Research Institute Symposia Series Volume XIV, Polytechnic Press, Brooklyn, New York; 1964.

76. P. K. Tien, J. P. Gordon, and J. R. Whinnery, "Focusing of a Light Beam of Gaussian Field Distribution in Continuous and Periodic Lens-Like Media", Proc. IEEE 53, 129 (1965).